Superoscillations: Photonic Technology Beyond the Diffraction Limit

[1,2)]Nikolay I. Zheludev and [2)]Guanghui Yuan

[1)] Optoelectronics Research Centre and Centre for Photonic Metamaterials, University of Southampton, Southampton SO17 1BJ, UK. E-mail: zheludev@soton.ac.uk

[2)] Centre for Disruptive Photonic Technologies, The Photonics Institute, School of Physical and Mathematical Sciences, Nanyang Technological University, Singapore 637371, Singapore. E-mail: GHYUAN@ntu.edu.sg

Abstract

The phenomenon of optical superoscillations first introduced in 2006 (J. Phys. A 39, 6965, 2006) and experimentally identified shortly after (Appl. Phys. Lett. 90, 091119, 2007) describes the rapid subwavelength spatial variations of intensity and phase of light in complex electromagnetic fields formed by interference of several coherent waves. Its discovery stimulated the intense revision of the limits of classical electromagnetism in particular the study of structure of superoscillatory fields in free space including unlimitedly small energy hotspots, phase singularities, energy backflow, anomalously high wavevectors and their intriguing similarities to the evanescent plasmonic fields on metals. In recent years, the better understanding of superoscillatory light has led to the development of superoscillatory lensing, imaging and metrology technologies. Dielectric, metallic and metamaterial nanostructured superoscillatory lenses have been introduced that are able to create hotspots smaller than allowed by conventional lenses. Far-field, label-free non-intrusive deeply subwavelength super-resolution imaging and metrology techniques that exploit high light localization and rapid variation of phase in superoscillatory fields have been developed including new approaches based on artificial intelligence. The present paper reviews the fundamental properties of superoscillatory optical fields and examines emerging technological applications of superoscillations.

Introduction

The phenomenon of superoscillations that we will explain below, challenges several commonly accepted wisdoms that have been living in the optics and electromagnetic research communities for generations. One of them is that a "band-limited" function spectrum of which contains no frequencies higher that B, cannot oscillate at frequencies faster than $2B$. The wisdom on "band-limit" has serious implications for optics, in particular to the resolution performance of optical instruments: the spot size of a perfect lens cannot be smaller than half of wavelength of light. This wisdom is also closely related to the Abbe diffraction limit: resolution of the best conventional microscope cannot exceed half the wavelength of light.

Moreover, in the view of diffraction limit it is often assumed that light fields in free space cannot change significantly on a scale smaller than half of the wavelength. This observation has been used intensely to justify the importance of plasmonics that allows highly confined electromagnetic excitations with large wavevectors at metal surfaces and therefore allows controlling light on the subwavelength scale [1,2]. Similarly, the diffraction limit of conventional optics has been the main stimulus to the research on metamaterial super-lens that should have allowed optical resolution beyond the diffraction limit by amplifying and conveying the large wavevector evanescent fields from the object to the image [3,4].

In fact, however, the phenomenon of superoscillations implies that for any fixed bandwidth, there exist finite-energy signals that oscillate arbitrarily fast over arbitrarily long time intervals, free space light can have deeply subwavelength structured features. In fact, Maxwell's electrodynamics allows light to be focused to a hotspot of any given size and resolution of optical microscopes is not limited to half of the wavelength. In this review, we will look at the manifestation of superoscillations in optics and will examine technological opportunities provided by this phenomenon, including optical imaging and metrology.

Functions that oscillate faster than the highest frequency in their Fourier Spectrum

As Berry & Popescu once noticed, functions can locally oscillate faster than their fastest Fourier component of the spectrum as in the Wigner representations the local Fourier transform can have both positive and negative values, which causes subtle cancellations in the Fourier integration over all of the function [5,6]. In other words, a function can oscillate fast within a limited segment in such a way that Fourier component of the function outside of the segment may cancel these high-frequency components.

Careful "engineering" of functions is required to achieve perfect cancellation. However, many examples of superoscillatory functions have been identified and several techniques have been developed to construct useful superoscillatory functions [5,7-16]. An example of such function with discrete spectrum $f(x) = \sum_{n=0}^{n=5} a_n \cos(2\pi n x)$, where a_0 =1, a_1 =13295000, a_2 =−30802818, a_3 =26581909, a_4 =−10836909, a_5=1762818. Near x=0, this function oscillates several times faster than its highest spectral component at frequency 10π [17].

This leads to a general definition: **Superoscillatory function is a function that locally oscillates faster than the highest Fourier component in the spectrum of the entire function.**

Superoscillatory function can also have continuous spectrum and such functions are often required for description of practical situations in optics. So-called prolate spheroidal wave functions [18] are very handy for this purpose and are often used to represent a superoscillatory function as a series of decomposition. Prolate spheroidal wave functions are band-limited in the spectral interval between -Ω and Ω, orthonormal on the interval [$-x_0$, x_0] and are exact zeros outside the boundaries of the spectral interval.

Figure 1 shows an example of a function with continuous spectrum $F(x) = A(x)\, e^{i\phi(x)} = 1.8126 \times S_2 + S_3$ that is constructed from just two circular prolate spheroidal functions S_2 and S_3 exhibiting the main characteristic features of superoscillatory functions:

- Band-limited nature. The highest frequency in the spectrum of $F(x)$ is π, see its spectrum in Fig. 1d, blue solid line.
- Fast local oscillations. Around $x=0$ function F(x) oscillates more than two times faster than the highest frequency component of its spectrum (compare solid blue line with dashed red line), and periods of the oscillations, Fig. 1b.
- Low amplitude of fast local oscillations**.** The amplitude of a superoscillatory function increases rapidly outside the superoscillating segment, Fig. 1a & b.
- Rapid phase variations. The phase $\phi(x)$ of the function (solid blue curve, Fig. 1c) changes very fast near the low-intensity regions where the speed of phase variation (dashed black curve, Fig. 1c) exceeds the speed of phase variation of the highest harmonic in the spectrum, $|\frac{\partial \phi(x)}{\partial x}| > \pi$.
- Broad local spectrum. Spectrum of the central part of the function is much broader than spectrum of the entire function, compare the dashed red line and solid blue line in Fig. 1d. Note that spectrum of the entire function in the interval $[-\infty, \infty]$ is bandwidth limited to ±π, while the central part has a much broader spectrum explaining the faster oscillation in the interval [-0.52, 0.52].

Properties of superoscillatory functions have been studied intensely in particular by Kempf and co-authors [10,19-21] who found that for a one-dimensional superoscillatory function the required energy grows exponentially with the number of superoscillations, and polynomially with the reciprocal of the bandwidth or the reciprocal of the superoscillations' period.

The information theory studies show [19,22] that for any fixed bandwidth, there exist finite energy signals that oscillate arbitrarily fast over arbitrarily long-time intervals, but these localized superoscillatory transients can only occur in signals that possess amplitudes of widely different scales. The existence of superoscillations and the possibility of encoding arbitrary amounts of information into an arbitrarily short segment of a low-bandwidth signal do not contradict the basic laws of information theory according to the Shannon theorem [23], as the superoscillatory information compression demands that the signal power grows exponentially with the amount of compressed information, i.e., with the length of the superoscillatory part of the message.

Superoscillatory focusing of light

In quantum physics, phenomena relevant to superoscillations have been discussed theoretically by Aharonov *et al.* from 1988 who noticed that the weak measurement of a quantum system can result in expectation values much higher than the spectrum of the operator [24,25]. Superluminal velocities in evanescent optical fields [26], random waves [27] and displacement of beam resulting from a slight change of polarization state due to spin-hall effect of photons [28] are manifestation of this phenomenon.

However, most importantly in optics the phenomenon of superoscillations offers the opportunity to focus light into a two-dimensional sub-diffraction hotspot smaller than ever possible with a conventional lens, focusing ability of which are limited by the Abbe "diffraction limit". According to Abbe, size of the hotspot of conventional lens δ is limited by $\delta = \lambda/(2NA)$, where $NA<1$ is the numerical aperture of the lens (see definition of *NA* below) and λ is the light's wavelength in the propagation medium. Therefore the smallest possible hotspot created by a lens is $\delta = \lambda/2$.

Similarly, the phenomenon of superoscillations allows achieving resolution higher than Rayleigh limit prescribed to conventional microscopes, a distance $\Delta = 0.61\lambda/NA$ at which two points can be distinguished as individuals. At this distance, the first dark ring of the Airy disk of the first point overlaps with the maximum of the other and the minimum intensity on the line between the points is 26% lower than the maximum.

The ability to focus light into a hotspot smaller than the "diffraction limit" was first noted by Toraldo Di Francia[29] with reference to earlier work on super gain (super-directive) antennas [30]. The focusing and imaging capabilities using Di Francia's phase masks were explored in the earlier works by the Technion group [31,32], but their relevance to the phenomenon of superoscillations discussed by Aharonov *et al.* [24,25] was not identified at that stage.

In a paper published on 16 May 2006, M. V. Berry and S. Popescu theoretically predicted that superoscillations can be realized in classical optics when a periodic diffraction grating produces superoscillations in a propagating beams without evanescent waves [5]. The first work that linked experimentally observed small light localizations and linked them to superoscillations was reported by Southampton University group in a paper published in 2007 [33]. It demonstrated that the quasicrystal array of nanoholes in a metal screen can "focus" light at distances of several tens of wavelengths from the screen, where subwavelength spots were formed without evanescent waves. This was a peculiar realization of Superoscillatory Lens, or SOL. The array produced superoscillatory foci of energy concentration in the "focal plane", harvesting light with a variety of transverse wavevector components emerging from a large number of holes in the array with a continuous spatial spectrum. These hotspots were mapped by scanning across the "focal plane" with a field probe, a tapered fibre probe with subwavelength optical aperture at its end. Colourful 'photonic carpets' were observed with a conventional optical microscope focused at different heights above the quasi-periodic nanohole array illuminated with a white light source [34].

The next significant step in the experimental study of superoscillations was the realization that superoscillatory hotspots can be directly imaged by a conventional optical microscope with high amplification [34]. Indeed, as the superoscillatory features are formed by free-space waves away from the diffraction mask, their spatial spectrum contains no evanescent components and is band-limited to the free-space wavevector. Consequently, imaging of these features can be achieved with a conventional optical instrument whose angular spectrum bandwidth is higher than that of the superoscillatory field generator. The numerical aperture of the optical instrument (NA_i) should be higher than that of the superoscillatory field generator (NA_S). The latter can be evaluated from the size D of the mask generating the superoscillatory hotspot and the distance F at which the hotspot is created as follows $NA_S = \sin\theta = \frac{D}{\sqrt{4F^2+D^2}}$ (see Fig. 2b). This work also predicted that superoscillations "may provide a new way to achieve subwavelength imaging in the far-field, different from the approaches based on the recovery of evanescent waves".

It was later shown that a subwavelength focus of *any size and shape* in an area beyond the evanescent fields can be created by diffracting a plane coherent wave on a dedicated mask with continuous variation of optical density and phase retardation [9]. An explicit recipe for the mask design includes the following steps: a) To decide on the desired hotspot size and profile in the focal plane. In principle, any size of the hotspot is possible (bear in mind that proportion of energy that can be focused into the hotspot reduces polynomially with the hotspot size [20]); b) To approximate the desired hotspot by a series of prolate spheroidal wave functions within a limited interval

known as the field of view (this is possible as the functions make an orthonormal set); c) To back-propagate the hotspot field from the focal plane to the plane of the mask (this is possible since the functions of the series are band-limited); d) The required spatial variation of the field intensity and phase are now known in the plane of the mask after back-propagation. Therefore, the spatial profile of its optical density and phase retardation of the mask can now be defined accordingly, to accommodate for structure of the incident wavefront.

An elegant method of constructing a range of superoscillatory hotspot by interference of only two prolate spheroidal wave functions is described [35]. We will illustrate the main characteristics of scalar two-dimensional superoscillatory hotspots at wavelenghth λ constructed by two prolate spheroidal wave functions $F(r) = A(r)e^{i\phi(r)} = 0.2291*S_4(r)+S_5(r)$ and formed by a mask with numerical aperture NA=0.9, Figures 1(f-i). The main characteristics here are similar to that of a one-dimensional superoscillatory function, Figure 1(a-e): The superoscillatory hotspot is smaller than focus of a conventional lens, but only a fraction of light's energy is concentrated in the superoscillatory hotspot, Figure 1(f); The hotspot is surrounded by concentric zones of rapid phase variation of phase φ where the local wavevector $k_{loc} = \frac{\partial \varphi}{\partial r}$ is larger than the amplitude of the wavevector in free space $k_0 = \frac{2\pi}{\lambda}$, Figure 1(g); The spatial spectrum of the entire hotspot including "halo" (the area surrounding low-intensity zone near the hotspot) is band-limited, Figure 1(h), while the hotspot itself has a much broader spectrum, Figure 1(i).

On account of polarization properties of light, the structure of superoscillatory hotspot becomes more complex, which is especially noticeable for superoscillatory fields with high numerical aperture (see Supplementary Materials Fig.1S). To mitigate for polarization conversion during focusing, in metrology and imaging applications of superoscillatory detectors, polarization filters are often used.

Here it should be noted that, superoscillatory focusing into the hotspot of arbitrary small size is only possible for the central hotspot of the intensity distribution. If the full extent of the light intensity distribution at the focal plane is taken into account, the generalised "common sense" Abbe criterion still stands in terms of the spot size into which 50% of the incident power can be focused [36]. Superoscillatory focusing is also compatible with the limitations of the uncertainty principle [37], when the broadened spectrum of the central hotspot is taken into account. However, we will see below that bandlimited nature of the hotspot and rapid phase variation in its vicinity open opportunities for high-resolution optical metrology and deeply subwavelength imaging.

Technologies of superoscillatory lenses

Multi-foci SOLs. From the earlier stage of research on optical superoscillations, it became clear that superoscillatory hotspots could be used for imaging. Coherent light diffracted by a quasicrystal array of nano-holes in a metal screen creates a complex volume distribution of hotspots, Figure 2a. Such array of holes can act as an elementary multi-foci lens imaging light emanating from the end of a tapered fiber to a screen at the image plane: upon moving the fiber end the superoscillatory hotspot moves in the opposite direction on the imaging plane, as appropriate for a convex lens creating a real inverted image of the object [38]. Although multiple foci in the imaging plane are advantageous for some imaging modalities [39], majority of applications require lenses with a single hotspot.

Continuous profile SOLs. A mask with precisely engineered continuous variation of transmissivity and retardation can create a superoscillatory focus of any size or shape [9]. For photonics applications, masks with radial symmetry are often used. Typically, the small hotspot created by the mask at the focal plane is surrounded by a "halo" – an intense ring of light. The diameter of the superoscillatory "field of view", the low-intensity area between that hotspot and the halo is important: larger fields of view simplify applications. However, manufacturing a mask with precisely engendered gradients of transmissivity and retardation is a formidable challenge. Recently an advanced photolithography was demonstrated to create a grayscale density superoscillatory lens. The technique uses femtosecond laser pulses to induce phase-change transitions in a thin layer of material that locally controls the exposure dose to photoresist, thus allowing a three-dimensional sculpting with grey scale density variation and submicron lateral resolution [40]. However, so far superoscillatory lenses with simultaneous continuous grayscale variation of optical density (transmission) and optical thickness (retardation) have not yet been demonstrated.

Binary SOLs. Currently majority of superoscillatory lenses are constructed with binary intensity or phase masks. A binary mask is a pattern in which either optical density or phase retardation can take two fixed values,

transparent-opaque in case of intensity masks or a 180° phase difference for the phase masks. No analytical expressions are known for reverse designing of binary masks. Instead, the particle swarm optimization technique has been widely employed [41-46]. Typically, the merit functions for optimization include the size of the central spot, numerical aperture, and size of the usable field of view. Similar approach is used for designing binary phase masks. Evolutionary[47] and genetic algorithms [48-51], optimization-free methods [52,53], and artificial intelligence algorithms are also being used for superoscillatory binary lens design.

By construction, the binary masks resemble Fresnel zone plates but are much more complex. Binary intensity masks are either concentric arrays of holes [54,55] or a "matryoshka" arrangement of concentrically enclosed slits in an opaque screen, typically a metal film [41,44,56,57], Figure 2c. Binary intensity superoscillatory lenses have been demonstrated at flat substrates, at ends of large mode diameter photonic crystal fibers [58], GRIN lenses and by structuring atomic thin layers of chalcogenide semiconductors [59]. The step-type phase masks have been fabricated in silicon and silica by optical lithography [60,61], while rewritable and reconfigurable superoscillatory lenses have been demonstrated using phase change materials [62].

The most advanced binary phase superoscillatory lenses were fabricated in a CMOS compatible high-throughput optical lithography process on a large silica wafer [60]. They were optimized for the wavelength of 633 nm, having diameter of $2R$=1.2 mm and focal distance of F=200μm. An ideal conventional singlet lens with such parameters would have NA = $\frac{R}{\sqrt{F^2+R^2}}$ = 0.95 and will focus into a hotspot of δ= 335nm = λ/(2NA), or δ= 0.53λ. The superoscillatory lens focuses light into the hotspot of δ_{SOL} = 253 nm, or 0.4λ, i.e. a quarter smaller.

Here we can introduce the effective numerical aperture of the superoscillatory lens as NA= $\lambda/(2\delta_{SOL})$ = 1.25. Such effective numerical aperture can only be achieved with superoscillatory lenses. It is not possible to reach NA ≥ 1 with a conventional lens or gradient metasurface lense[63,64] focusing in free space. Conventional high numerical aperture lenses are often complex and usually very expensive (thousands of dollars), while quartz phase SOLs are flat, simple in construction and cheap in production. Quartz phase SOLs have negligible absorption loss and can sustain high light intensities. Immersion, in particular solid immersion, i.e. placing a layer of high refractive index dielectric between the lens and the focal plane reduces the size of the hotspot even further [65,66]. Obvious shortfalls of the SOLs are presence of halo and low throughput efficiency into the hotspot that limits some applications such as light-assisted manufacturing.

"Optical needle" SOLs. Often the superoscillatory lens design is optimized to achieve a small hotspot at a particular distance from the mask. However, many applications including data storage, metrology and manufacturing with light benefit from long depth of focus. Depth of focus (*DOF*) of a conventional lens[67] is linked to its numerical aperture $DOF \sim \lambda/NA^2$: the larger is *NA*, the smaller is the hotspot, the shorter is the depth of focus and for high NA lenses DOF ~ λ.

Channelling light into a radiation 'needle stick' was discussed with reference to Albert Einstein's "Einsteinschen Nadelstichstralung" about a hundred years ago [68]. Remarkably, binary SOLs can be engineered to produce these 'needle stick' a hotspot with very long depth of focus along the axial direction in such a way that at any cross-section the hotspot remains smaller than the "diffraction limit" allows. Such light patterns were termed "optical needles" [69-73], Figure 4d. Optimization of "optical needles" can involve blocking the central part of the lens thus preventing nearly coaxial diffracted waves to reach the focus. For example, a sub-diffraction binary intensity circularly polarized optical needle generator with a transverse spot size of 0.45λ and axial depth of focus of as long as 15λ has been demonstrated at a violet wavelength of 405 nm [71].

The optical needle lenses have the potential applications in high-density optical storage and heat-assisted magnetic recording. Heat-assisted magnetic recording (HAMR) is a data storage technology to overcome the superparamagnetic limit in high density magnetic recording. Existing HAMR schemes depend on a simultaneous magnetic stimulation and light-induced local heating of the magnetic information carrier. To achieve high-density recorded data, near-field plasmonic transducers have been proposed as light concentrators [74]. Superoscillatory solid immersion lens offers an alternative approach exploiting a far-field focusing device that can focus light into sub-50 nm hotspots in the magnetic recording layer using a laser source operating at 473 nm [75]. Such a lens, a combination of SOL with solid immersion, has an effective numerical aperture as high as NA=4.17. Similarly, superoscillatory lenses may be used for readout of optical memory with pitch between data marks less than λ/4 this offering high density data storage not accessible with conventional lenses [54].

Binary SOLs are fabricated using standard nanofabrication approaches: focused ion beam (FIB) milling, electron beam lithography (EBL), photolithography and etching. FIB is the simplest way to fabricate binary-amplitude SOLs. After depositing a thin layer of metal films on a transparent substrate, the film is directly milled by FIB to remove those parts of the mask that are to transmit light. In general, harder metals, such as chromium or titanium, take longer to mill in the FIB, but give better fabrication quality.

Achromatic SOLs. Superoscillatory lenses typically create a chain of foci along the lens axis. Position of foci on the axial line depends on the wavelength of light and multiple foci at different wavelength can overlap. SOLs have been engineered in such a way that one of these foci on a particular wavelength overlaps with another foci at a different wavelength so superoscillatory hotspots are achieved at the same focal distance for two different wavelengths, Figure 2e. This creates an achromatic superoscillatory lens. Simultaneous focusing of three different wavelengths (Red-Green-Blue) on one sub-diffraction hotspot has been demonstrating creating a white-light apochromatic superoscillatory lens [58]. We anticipate that achromatic and apochromatic sub-diffraction SOLs could serve as super-resolved focusing and imaging tools for a broad range of applications in nonlinear spectroscopy, photography, retinal diagnostics, low-cost fiberized microscopy, high-resolution quantum correlation measurements, pump-probe experiments for ultrafast dynamics, excitation and collection of photoluminescence, coherent anti-Stokes Raman scattering for super-resolution bio-imaging, nonlinear imaging and nanofabrication using two/three-photon absorption.

Metamaterial SOL. Photonics community is well aware of the metamaterial super-lens which uses a slab of negative index metamaterial to recover evanescent waves from the object in the image plane. This powerful idea is not yet implemented as a practical imaging device and its realization in the optical part of the spectrum faces a number of challenges. However, the metamaterial approach is a practical way of creating a different type of super-lens that does not use evanescent waves but instead creates superoscillatory foci in the far-field from the lens. We call it the superoscillatory metamaterial lens (SML), Figure 2f.

The main advantage of the metamaterial approach is that, the nearly complete design freedom on transmissivity and retardation of the lens mask can be achieved using a metasurface. In such a lens, light is scattered on a planar array of "metamolecules", individual scatterers providing the prescribed levels of phase delay and scattering amplitude at different radial positions on the lens in such a way that the entire array diffracts light into a superoscillatory hotspot. It was recently demonstrated that, plasmonic metamaterial superoscillatory lenses allow reaching sub-diffraction hotspots on large field of views up to 6λ in diameter and robustly perform in imaging applications [76]. A metamaterial superoscillatory lens with effective numerical aperture NA=1.52 and focus as small as 0.33λ in size has been demonstrated. It contains 8500 metamolecules forming a lens of 40 μm in diameter.

To design such a lens, firstly a planar continuous gradient amplitude and phase mask necessary to transform an incident plane wave into a complex wavefront converging into the desired focus was calculated, as described above in the section "Superoscillatory focusing of light". Secondly, a library of subwavelength plasmonic metamolecules with individual scattering characteristics mimicking and matching the amplitude and phase characteristics found anywhere on the continuous mask was defined. Thirdly, the mask was simplified as a discrete metasurface, an array of metamolecules in a concentric pattern of metamolecules with characteristics tailored to provide the same attenuation and retardation as the continuous mask in the point of their location.

Each metamolecule was a V-shaped nanoslit cut into a thin gold film, a design that can be easily adjusted to control the polarization state, intensity, and phase of the scattered wave by adjusting length, opening angle of the V shape, and width of the slits [77,78]. The metasurface pattern was designed for linearly polarized incident light and acted as a SOL for transmitted light with orthogonal polarization. SMLs allow reaching smaller hotspots with better throughput efficiency than binary masks. They can be manufactured by well-established nano-manufacturing techniques and are scalable to operate at any wavelength. Other types of superoscillatory metasurfaces based on geometrical phase modulations for broadband focusing have also been demonstrated [79,80]. The simplest form of a binary metamaterial superoscillatory lens is a cylindrical SOL [81].

Single photon regime of SOL. Applications of SOLs in quantum super-resolution imaging, quantum lithography and bio-medical imaging often require low light intensity and question emerges whether superoscillatory focusing is possible in a single photon regime. This question is, in fact, relevant to the cornerstone question of wave-particle duality of photon: will the Young's double slit diffraction experiment work in a single photon regime, one photon at a time? [82] The studies of SOL performance in a single photon regime were undertaken

with a cylindrical metasurface superoscillatory lens [81]. The superoscillatory hotspot observed in the single-photon regime by detecting a pattern created by a large number of individual photons at the focal plane was the same as created with coherent laser illumination. This experiment proved a direct evidence that wavefunction of a single photon can superoscillate and contains sub-diffraction features with length scale smaller than that is constructed with allowable wavevector eigenvalues, thus linking the classical [25] and quantum [24] manifestations of the phenomenon of superoscillations.

Although binary masks provide a robust and simple way to implement subwavelength hotspot generators, they provide static superoscillatory fields. Superoscillatory focusing could also be achieved with spatial light modulators (SLM) creating a beam with carefully designed amplitude and phase profile for precisely tailored interference.

Double SLM superoscillatory generator. Precise programmable shaping of the beam may be achieved with a pair of analogue liquid crystal SLMs, one of which controls the phase profile of the beam and the other controls its intensity profile. The modulated beam is then imaged onto the back focal plane of the microscope objective. In this way, any arbitrary field profile may be obtained at the microscope focal plane simply by encoding its Fourier spectra on the SLMs. For review of the technology see Refs. [83,84] and for details on its implementation, see Ref. [85]. The double SLM technology is robust and apart from imaging applications (see below) it is used for atom trapping in cold atom experiment, see Figure 2S-a,b in Supplementary Materials. Superoscillatory focusing has also been used in other high-resolution optical trapping and manipulation applications [86,87], where the trapping potential provides unprecedented localization accuracy and stiffness, significantly exceeding those of conventional diffraction-limited beams.

Digital Micromirror superoscillatory light generator. Full control of the phase and intensity can also be achieved with a single binary spatial light modulator based on the Digital Micromirror Device (DMD), see Figure 2S(c). A DMD chip is a micro-opto-electromechanical system that has millions of microscopic mirrors on its surface arranged in a rectangular pixilated array. Such chips are widely used in digital image projectors. The mirrors, typically 16 μm across, can be individually switched on torsion hinges by electrostatic force between two orientations corresponding to "on" or "off" state, Figure 2S(c). The method for generating beams with arbitrary phase and intensity profiles is termed 'digital holographic grating' [88,89], where a computer-generated hologram is designed and loaded as a binary mask on DMD carrying the amplitude and phase information of desired light beam. The first-order diffraction on this holographic grating is the target light beam, which is designed as a superoscillatory hotspot.

SOL vs SLM. SLM superoscillatory focusing has a number of experimental differences to focusing with binary static superoscillatory lenses. The SLM approach allows focal spots to be formed at the focus of a microscope objective, giving a working distance of at least a few hundred microns, compared to the few tens of microns typically achieved with static binary superoscillatory lenses. SLM superoscillatory focusing can also be combined with active scanning of the hotspot across the object by controlling the beam direction with SLMs. However, the SLM system is more complex to align, consisting of a number of optical components and has considerable physical dimensions in comparison with static SOLs having only one component that is relatively easy to align with input laser.

THz and acoustic superoscillations. The studies and development of applications of superoscillations is now extended to the terahertz electromagnetic frequency range [47,90,91]. A superoscillatory metalens with a resolution below the diffraction limit is demonstrated working around 0.327 THz [47]. A THz far-field sub-diffraction optical needle for a wavelength of 118.8 μm with focal length 420λ and radius 160λ has been demonstrated for applications in super-resolution THz tomography [90]. An ultrasonic binary superoscillatory lens has been developed for super-resolution ultrasound imaging and tweezing application [92,93].

Superoscillations in complex fields

Although dedicated superoscillatory field generators and SOLs can create prescribed hotspots, superoscillations, in fact, commonly appear in complex light fields [94,95]. Importantly, complex electromagnetic field structures created by interference of multiple coherent light waves can have deeply subwavelength features in their structures.

Following Ref. [96], this can be illustrated by example of a light field $U(r) = U_0(\boldsymbol{r})\, e^{i\varphi(\boldsymbol{r})}\, e^{i\omega t}$ created by interference of 50 coherent plane waves oscillating at frequency ω with random amplitudes and phases and

propagating in the plane with prevailing direction of propagation along $\boldsymbol{k}_{||}$, from left to right, Figure 3: $U(r) = \sum_{i=1}^{i=50} A_i e^{i\omega t - \boldsymbol{k}_i \boldsymbol{r}}$, $\boldsymbol{k}_{||} >> \boldsymbol{k}_{\perp}$. Figures 6 shows a fragment of this field pattern that is 4λ x 4λ in size.

A color-coded map of the phase $\varphi(\boldsymbol{r})$ of the resulting light field is presented in Figure 3a. Here circles indicate singularities, points on the map where phase of the wave is not defined. Black and white circles indicate singularities of two different types. If by circling around the singularity clockwise the phase increases, a white circle with black core is used; if by circling around the singularity clockwise the phase decreases, a black circle with white core is used.

Figure 3b shows the color-coded map of intensity $U_0(\boldsymbol{r})$ of the light field. Note that singularities are located where intensity goes to zero. The map features a few energy localization hotspots. Some of them are smaller than that is allowed by the "diffraction limit". For instance, the hotspot enclosed by the dashed white line is only 0.31λ in the transverse direction. While the overall energy flow is from left to right, the light field also contains zones of energy backflow (EBF) coloured in brown. In the energy backflow zones, the predominant direction of the Pointing vector of light is opposite to the predominant direction of light propagation in the beam and this can be often seen in complex superoscillatory fields. Note that energy backflow zones are often much smaller that the wavelength of light. It has also been noticed that perimeter of the energy backflow zone contains the phase singularity point and the tangential to the perimeter at this point is directed parallel (anti-parallel) to the prevailing direction of energy flow [96].

Figure 3c shows the color-coded map of intensity $U_0(\boldsymbol{r})$ overlapped with maps of the zones where phase of the field changes rapidly perpendicular to the prevailing direction of propagation, along $\boldsymbol{k}_{\perp}$, i.e. where $|\nabla\varphi(\boldsymbol{r})_{\perp}| > |\boldsymbol{k}|$. Note that narrow areas of these zones (waists) coincide with positions of singularities. The value of $|\nabla\varphi(\boldsymbol{r})_{\perp}|$ reaches local maxima at the narrow waists, around the singularity points. These zones are deeply subwavelength in size and the maxima of $|\nabla\varphi(\boldsymbol{r})_{\perp}|$ are highly localized at singularities.

We will see below that these subwavelength features of complex coherent electromagnetic fields can be used in super-resolution metrology and imaging, but before that we shall describe how these features can be mapped experimentally.

Mapping superoscillatory field with deeply subwavelength resolution

In spite of the intense interests in the subject of optical superoscillations for many years, experimental evidence of large local wavevectors and energy backflows in superoscillatory optical fields – some of their main features - was only reported recently [97]. Observing these features in optics is much more complex than demonstrating the intensity hotspots. Such observation needs the capability to measure not only amplitude of the optical field, but also its local wavevectors $\boldsymbol{k}_{local} = \nabla\varphi$, and hence the phase φ of the field. As the phase information can only be obtained in interferometric measurements, extreme stability of the interferometer is needed to acquire reliable data on the fields with small spatial features and fast phase variations. As the superoscillatory fields are expected to have spatial features that are much smaller than the wavelength of light, spatial resolution far better than allowed by the Abbe-Rayleigh limit of half-wavelength is required. To meet these challenges, a monolithic metasurface interferometry technique has been developed [97], see Figure 3S, Supplementary Materials. In this technique, the superoscillatory field under investigation and the reference wavefront needed for interferometry are created by the same mask (planar metamaterial nanostructure), i.e. on the same monolithic platform, thus minimizing the instability and alignment problems characteristic for bulk free-space interferometers.

Resulting field maps in the vicinity of a superoscillatory hotspot reveal four main characteristic features of superoscillatory fields obtained experimentally and computationally (see Figures 4b):

1. Subdiffraction limit hotspots, Figures 4b and 3S(c). On the intensity map (~ $|E_y|^2$) the hotspot size in the x-section is smaller than allowed by the Abbe-Rayleigh limit. The focus is surrounded by fringes similarly to how focal spot of a conventional lens of finite size is surrounded by the oscillating Airy-type pattern. However, here the fringes are more densely spaced and are more intense;
2. Phase singularities, Figures 4b and 3S(d). The hotspots are flanked by phase singularities at the low-intensity regions near the focus (green circles, see the phase maps $\varphi = \arg(E_y)$). When moving along the loop encircling the phase singular points, the phase changes by 2π or - 2π, depending on the topological charge of the singularity m = +1, or m = -1, correspondingly.

3. Giant local wavevectors, Figures 4b and 3S(e). Magnitude of the local wavevectors $|k_x|$ far exceeds magnitude of the wavevector of a plane wave in vacuum, $k_0 = \omega/c$. Here the transverse local wavevector k_x as x-component of $\boldsymbol{k}_{local} = \nabla\varphi$. The $|k_x|$ near the phase singularity is more than an order of magnitude higher than k_0.

4. Energy backflow, Figure 4b and 3S(f). The field features have energy backflow zones where light's energy retro-propagates. These zones can be derived from the mapping of longitudinal wavevector k_z and they are pinned to phase singularities, as predicted in Ref. [96]. Maps of the time averaged Poynting vector $S = \frac{1}{2}\mathrm{Re}\{E \times H^*\}$ show that in these regions the incident energy flow is "trapped" and circulates without propagating in the forward direction (see insets to Figure 4b).

These maps are a powerful illustration of the fact that superoscillatory fields can have structured elements that are much smaller than prescribed by the Abbe-Rayleigh limit for lens-focused hotspot. Indeed, here the backflow areas are only about $\lambda/20$ in size along x-direction. Superoscillatory areas where $|k_x| > k_0 = \omega/c$ are even smaller, of the order of $\lambda/100$. This confirms Berry's observations that "the regions of backflow are considerably smaller than the wavelength" and that "in the neighbourhood of phase singularities wavefunctions can vary on sub-wavelength scales" [96].

"Plasmonics" in free space

The mapping of the intensity and phase profile near a superoscillatory focus have revealed some remarkable similarities between near-field plasmonic focusing by nanostructures and superoscillatory focusing in free space, Figure 4. Indeed, rapid spatial phase variation, giant local wavevectors and phase singularities are routinely observed in computational experiments on plasmonic nanostructures. Plasmonic fields do not propagate into free space, they are a collective excitation of electromagnetic fields and electrons in the evanescent area of the dielectric-metal interfaces with high magnitudes of wavevectors. In fact, the access to high-value wavevectors is what makes plasmonics a preferred platform for nanophotonic devices.

Similarities between the superoscillatory and plasmonic field are striking. For instance, Figure 4a shows a silver nanoparticle at plasmonic resonance [98]. One can see energy backflow zones pinned to singularities that resemble the structure of fields at the superoscillatory focus described in the previous section. Both in plasmonic and superoscillatory foci, zones of energy of backflow facilitate the subwavelength localization of light. They remove electromagnetic energy from the areas neighbouring the foci squeezing it.

Moreover, plasmonic and superoscillatory focusing seems to follow a similar scaling law: the energy throughput efficiencies scale polynomially with size of the focal spot. Indeed, a deeply subwavelength hole of diameter σ in opaque screen can be used as a nanoscale light source, for instance in scanning near-field optical microscopy. Only a small proportion of light illuminating the screen will pass through the hole. Here throughput efficiency scales as $\left(\sigma/\lambda\right)^4 + o\left(\sigma/\lambda\right)^4$. A small absorbing dielectric or plasmonic nanoparticle of diameter σ will also "focus" light by harvesting energy of the illuminating plane wave (see Figure 4a) with scattering cross-section that scales as $\left(\sigma/\lambda\right)^4$. Similarly, in the regime of superoscillatory focusing in free space, only a small fraction of light can be focused in the hotspot: the proportion of energy channelled into the superoscillatory region decreases polynomially $P\left(\sigma/\lambda\right)$ with size of the superoscillation [19,54].

Metrology with superoscillations

Light is a perfect tool for metrology as it allows non-disruptive measurements of the size or position of the object against a ruler (see Figure 5a). Displacement of the object against a ruler can be measured optically with the help of a conventional lens or microscope with resolution limited by diffraction to about half of the used optical wavelength λ, typically a fraction of micrometer. Various interferometric techniques that require complex and heavy equipment can also be applied to measure mutual displacement of macroscopic objects that essentially have the same fundamental limit to resolution when light's intensity is used in the measurements.

Since the deeply subwavelength features of complex electromagnetic fields can be mapped with high resolution (see section "Mapping superoscillatory field with deeply subwavelength resolution"), they can be used as reference points of a more precise ruler, Figure 5b. Indeed, it was shown that resolution three orders of magnitude better than the diffraction limit can be achieved by using – instead of the physical ruler – an "optical

ruler", the electromagnetic field structured at the deeply subwavelength scale [99]. The "optical ruler" metrology uses the fact that free-space optical fields can be imaged by a conventional lens with no limit to resolution and that the phase information can be retrieved by the monolithic metamaterial interferometry as show in Figure 3S, Supplementary Materials. The "optical ruler" can be used for measuring mutual displacement of two platforms, one containing a laser source and a metamaterial mask generating optical ruler and the other containing a magnifying lens, polarizer and image sensor, Figure 4b.

One- and two- dimensional displacement measurements are possible with the "optical ruler". For the one-dimensional metrology, the "optical ruler" light field is created by a one-dimensional Pancharatnam-Berry phase metasurface which is constructed as rows of slits oriented at +45° and -45° to the incident polarization. It is designed to create a superoscillatory focus of cylindrical lens flanked by singularities. For the two-dimensional metrology, the Pancharatnam-Berry phase metasurface is a regular two-dimensional array of slits with randomised orientation either at +45° or -45°. Such random metasurfaces create a superoscillatory speckle optical field. In both cases of one- and two-dimensional metrology the fields created by the metasurfaces are superoscillatory for polarization perpendicular to the polarization of the incident light. Upon transmission through the metasurface the light component with incident polarization remains a plane wave. By detecting the interference pattern of these waves through a magnifying lens and a polarizer for different polarizations of the incident wave, the full phase and intensity profile of the "optical ruler" can be retrieved with resolution of better than 1 nm using coherent light source at the wavelength of 800 nm [99].

The optical ruler metrology is a far-field technique and therefore allows for noncontact operation. The subnanometer resolving power of the optical ruler is higher than that of most optical super-resolution and interferometric techniques. It does not suffer from the mechanical and thermal instabilities that affect large conventional metrological interferometric instruments. The metasurface can be manufactured at the tip of an optical fiber, allowing numerous applications where high resolution, small size, and noncontact operations are essential, including monitoring displacements of scanning stages of atomic force microscopy, scanning tunnelling microscopy, and super-resolution optical microscopes, lithography mask alignment, and the control of motion of tools in nanoassembly. The optical ruler can also be placed on nanoindenter heads to measure the modulus of elasticity, yield stress, hardness, and wear resistance of materials. One can even envisage the optical ruler attached to a cutting tool of a smart manufacturing lathe or milling machine. Lastly, the optical ruler can be used for monitoring of mutual nanoscale displacements of parts of precision constructions, such as large optical telescopes, disc drives, microelectromechanical systems and nanoelectromechanical systems devices, acceleration sensors, and for monitoring the deformation, fatigue, or thermal expansions of components.

Shortly after the paper [99] was published, we received an interesting comment from M. V. Berry who put light on the earlier history of using singularities in metrology, in this case with radio waves [100] (private communication): "We discussed a possible application [of singularities]: measuring movement of polar ice sheets. The idea was to choose a place on the ice surface where the disorderly echo from the bottom displayed a phase singularity, wait overnight while the ice sheet moves, and then explore the surroundings to find a place where the echo was the same as yesterday. With radio waves of length 5m, the extreme phase sensitivity would enable displacements of a few cm to be detected."

Challenges of Imaging

The Abbe-Rayleigh diffraction limit of conventional optical instruments has long been a barrier to studies of microscale and nanoscale objects. The earliest approaches to overcome the limit were based on recording shape of the object by registering its optical near-field formed by rapidly oscillating but non-propagating waves with large wavevectors: contact photography and scanning near-field optical microscopy (SNOM).

In contact lithography, the near field is registered by the photographic emulsion placed in contact with the object. The emulsion is detached (pilled off) from the object after exposure to light leaving its photo-imprint in the emulsion. Unfortunately, contact photography offers no magnification to the level of detail that can be seen by naked eye. It is not suitable for super-resolution imaging. Having said that, its modern version, optical mask lithography with short wavelength light sources is extremely useful for semiconductor chip manufacturing and is widely used.

In the SNOM, a small aperture or scattering probe captures its evanescent field, converts it into propagating waves and directs to a photodetector. The technique can achieve subwavelength spatial resolution but requires

the probe to be scanned in the nanoscale proximity of the object. Its applications are limited as it cannot be used to image inside cells or silicon chips, for example, and image acquisition takes a long time.

A number of metamaterial-based techniques have been proposed to reconstruct and capture evanescent fields, most notably the far-field Veselago-Pendry "super-lens". In the super-lens, a slab of negative index metamaterial is used to image the evanescent waves from an object on to the imaging plane. This approach, however, faces substantial technological challenges in its implementation in optics, and has not yet been developed as a practical imaging technique. The super-lens provides imaging with no magnification which also limits its practical use.

Could deeply subwavelength resolution in imaging be achieved without detecting the near field? A classical approach for imaging uses conventional lens that focuses light scattered by the object into the imaging plane with magnification. This approach does not have any limits in magnification, at least in principle, but has a sharp limit on resolution of about half the wavelength.

Nevertheless, far-field super-resolution imaging is possible and in biological studies is dominated by the stimulated emission depletion (STED) and single-molecule localization (SML) microscopies [101,102] that require intense laser illumination and labelling samples with luminescence agents (e.g. semiconductor quantum dots). These labels are known to change the behaviour of the biological systems while labelling cannot be applied to solid artificial nanostructures (e.g. silicon chips) making these techniques unsuitable for nanotechnology use. The other major far-field super-resolution technique is structured illumination microscopy (SIM) when object is illuminated with periodically modulated light patterns. However this approach requires complex post processing and can only double the resolution of a conventional microscope.

Below we will review two approaches to far-field label-free super-resolution imaging techniques that use superoscillatory optical fields for sample illumination: "Confocal Superoscillatory Imaging" and "Deeply Subwavelength Topological Microscopy" enabled by artificial intelligence.

Confocal Superoscillatory Imaging

A route to far-field subwavelength imaging is using optical superoscillatory hotspot for illuminating the object. Microscopy with superoscillatory illumination of the object has been developed from 2012 [41]. It has been shown that resolution of confocal microscopy with superoscillatory illumination is determined by the size of the hotspot, while accrued images are themselves superoscillatory and hence can reveal fine structural details of the object that are lost in conventional far-field imaging. This microscopy is a non-algorithmic, low-phototoxicity imaging technology and is a powerful tool both for nanotechnology and biological research of samples that do not allow labelling, such as silicon chips and live cells.

A conventional microscope uses a powerful objective lens to project light scattered by the object to the image plane with magnification, where it is registered. Typically, an incoherent light beam with a homogeneous profile is used to illuminate the object. The spatial resolution of a conventional microscope is limited by the point spread function of objective lens and cannot exceed $\Delta=0.61\lambda/NA$, where λ is the wavelength of the light and NA is the numerical aperture of the lens (Rayleigh limit).

In principle, superoscillatory lenses can be used to image objects that are smaller than the field of view [41], but this has limited practicality [103]. For a broader range of applications the conventional microscope objective lens cannot simply be replaced with a superoscillatory lens: the images of the objects that are bigger than the field of view will be distorted by light scattering from the halo-illuminated parts. This can be mitigated in a confocal microscope when a conventional lens with high numerical aperture is used as the objective lens, while the sample is illuminated by SOL with tight focus. Imaging is achieved by scanning the sample relative to the focus of the superoscillatory lens with a small confocal aperture at the detector, that rejects most of scattering from the halo illuminated parts of the image.

How does this confocal microscope work? Let P_{SOL} and P_{COL} to be the point spread functions of the illuminating superoscillatory lens and conventional objective lens (see Figure 6(d)). The microscope's response is characterised by its point spread function $P_{\mathrm{MIC}} = P_{\mathrm{SOL}} \times P_{\mathrm{COL}}$ and it is bandlimited to spatial frequency $\Phi = 2\pi \times \mathrm{NA}/\lambda$, where NA is the average of the numerical apertures of the illuminating lens (SOL) and the imaging lens (COL)[85]. If the object has subwavelength structures and the function $O(\boldsymbol{r})$ describing it is not

bandlimited to Φ, a conventional microscope cannot resolve its fine details beyond $\frac{\lambda}{2\mathrm{NA}}$. However, the image $I(\boldsymbol{r}) = P_{\mathrm{MIC}} \otimes O(\boldsymbol{r})$ created by the superoscillatory microscope is different ($\otimes$ denotes a convolution): it is a superoscillatory function and can therefore locally oscillate much faster than Φ and can contain detail finer than $\lambda/(2\mathrm{NA})$. A mathematical example of forming superoscillatory image in such band-limited system is presented in Ref. [85]. Therefore, the main principle of superoscillatory microscopy is that superoscillatory illumination creates a superoscillatory image and a band-limited system is used to achieve this.

A superoscillatory microscope can be constructed by adding a laser-based superoscillatory illumination system to a conventional confocal microscope. Such a microscope was first demonstrated in 2012 using binary transmission mask as superoscillatory illuminating lens and a laser operating at the wavelength of 640 nm. It resolved nanoscale slits in an opaque screen spaced by a distance of 137 nm and round holes spaced by a distance of 105 nm (0.16λ). The slits were completely unresolved if conventional illumination was used in the same microscope.

The first use of metamaterial superoscillatory superlenses in imaging applications was reported in Ref. [76]. In this work, the dependence of the superoscillatory microscope resolution on the size of superoscillatory hotspot was investigated: the resolution steadily follows the size of the hotspot, the smaller the sub-diffraction hotspot, the better the resolution. With a superoscillatory hotspot of 264 nm (0.33λ), pairs of 160 nm holes in a metal film separated by 120 nm (0.15λ, edge to edge) were comfortably resolved with superoscillatory illumination using a laser source operating at the wavelength 800 nm.

The first use of dielectric binary superoscillatory superlenses manufactured from quartz using CMOS compatible lithography was reported in Ref. [60]. With a laser source at wavelength 633 nm patterns and pairs of holes spaced by a distance of 110 nm (0.17λ, edge to edge) have been resolved with superoscillatory illumination that conventional bright-field imaging modality was not able to resolve.

A sophisticated microscopy using superoscillatory illumination was demonstrated in Ref. [85] [104] reporting high-frame-rate polarisation-contrast imaging of unmodified living cells with resolution significantly exceeding that achievable with conventional instruments. This work demonstrated that this non-algorithmic, low-phototoxicity imaging technology is a powerful tool for biological research. In contrast to confocal superoscillatory microscopy with static superoscillatory lenses, superoscillatory illumination was achieved with spatial light modulators: the fixed static binary superoscillatory lens was replaced with a system of spatial light modulators to illuminate the sample. The bio-version of confocal superoscillatory microscope also incorporated a liquid crystal polarisation controller to implement an advanced form of polarisation contrast imaging, giving high contrast even in unstained transparent biological samples, Figure 6.

It is educational to compare superoscillatory confocal microscopy with stimulated emission depletion (STED) microscopy. STED functions by depleting fluorescence in specific regions of the sample while leaving a central focal spot active to emit fluorescence. In contrast, superoscillatory confocal microscopy functions by illuminating the sample locally with a superoscillatory lens. Both are far-field super-resolution techniques, but STED requires labelling of the sample with a fluorescent reporter while superoscillatory microscopy works with unlabelled samples. Superoscillatory confocal microscopy is a linear imaging technique working at low light intensities while STED is a nonlinear optical technique that requires intense laser radiation to deplete the fluorescence around the central focal spot.

Deeply Subwavelength Topological Microscopy

The far-field confocal superoscillatory imaging described above has been proven to work in a variety of applications and in particular, it offers video-frame-rate high-resolution microscopy for demanding bio-imaging tasks [85]. However, since the intensity of the superoscillatory hotspot rapidly drops with the hotspot size (while the interference from the halo increases) the signal to noise ratio goes down for smaller hotspots and higher levels of resolution. In a conventional confocal microscopy setting, it is practically difficult to reach resolution beyond λ/5 using superoscillatory illumination.

Can resolution of imaging with superoscillatory illumination be improved beyond this point and reach a deeply subwavelength resolution? Recently, two ideas have been explored to make it possible.

The first idea comes from the observation that in the confocal imaging mode, light scattered on the sample is detected through an aperture and the rest of scattered field is blocked. Could the rejected light be useful to

construct a better resolved image of the sample? Indeed, different iterative feedback algorithms have been developed enabling the reconstruction of an image from intensity of scattering patterns of optical, deep UV and X-ray radiation with resolution essentially limited by the wavelength of the illuminating light in most cases [105] and around 5-times higher when compressed sensing techniques for imaging sparse objects are used [106].

Artificial intelligence in the form of deep learning is a powerful methodology for solving ill-posed inverse problems [107-110]. Indeed, recently an artificial-intelligence enabled microscopy was introduced, which reveals the fine structure of an object by analysing its far-field scattering pattern. The object is reconstructed from the intensity profiles of scattered light while the reconstruction is performed by a neural network trained on a large number of scattering events. This technique was termed Deeply Subwavelength Optical Imaging and has been demonstrated experimentally by imaging dimers with subwavelength features with resolution exceeding $\lambda/20$ [111]. Later this technique was applied to imaging subwavelength slits in opaque screen and resolution of $\lambda/800$ has been achieved experimentally bringing it to sub-nanometer resolution [112]. So, the first idea is using deep learning to solve the inverse scattering problem of imaging.

This brings us to the second idea. Could deeply subwavelength features of superoscillatory fields such as zones of rapid variations of phase and energy backflow zones be exploited for high-resolution imaging? In essence, can we reach and exceed the level of optical imaging resolution to the nanometric level achieved in "optical ruler" metrology (see section "Metrology with superoscillations" above) using the topological features of light such as singularities?

Figure 7(b)-(c) illustrate the sensitivity of the scattered field pattern on placing a small absorbing nanoparticle only $\lambda/1000$ in size, in the topologically structured field[99,113]. It follows these figures and from Ref. [97] that scattering of the superoscillatory field is two to three orders more sensitive than in the case of plane wave illumination to the presence and repositioning of the nanoparticle, which we attribute to the presence of high intensity and phase gradients in the superoscillatory field. Indeed, placing or displacing in the very narrow subwavelength singularity zone (black horizontally extended area indicated by green dotted line) results in a strong change of intensity across the detector plane. The Deeply Subwavelength Topological Microscopy (DSTM), Figure 7, with superoscillatory light was recently demonstrated[113] that reveals the fine structure of an object through its far-field scattering pattern under illumination with light containing deeply subwavelength singularity features. The object is reconstructed by a neural network trained on a large number of scattering events on objects with known characteristics. In numerical experiments on imaging of a dimer, resolving powers better than $\lambda/200$, i.e. two orders of magnitude beyond the conventional "diffraction limit" of $\lambda/2$, has been demonstrated. Proof-of-principle experimental confirmation of DSTM with a training set of small size, yet sufficient to achieve resolution five-fold better than the diffraction limit have also been reported. There are several factors contributing to high resolution of DSTM:

1. From the prospective of Fourier optics and theory of superoscillations, topological illumination with superoscillatory light gives access to high local wavevectors and ensures much higher sensitivity of the pattern of scattered light to small features of the imaged object than unstructured light;

2. From the prospective of the information theory, recording of multiple scattering patterns during the training process and imaging provides much more information on the imaged object for the retrieval process than what is available in the lens-generated single image for which the Abbe limit has been derived;

3. Sparsity of the object and prior knowledge about the object shall also be a helpful factor in imaging simple objects such as a dimer, as this helps the retrieval process, similarly to how sparsity helps 'blind' compressed sensing techniques;

4. The deep learning process involving a neural network trained on a large dataset creates a powerful and accurate deconvolution mechanism without using explicit information on the phase of the detected signals. Experiments show that larger training sets give higher resolution.

An interesting direction for future research could be the analysis of resolution limits of microscopies using prior knowledge of the sample and deep learning artificial intelligence techniques that give access to the large amount of information accrued during the neural network training process. This gives an advantage over conventional

single short imaging: From the prospective of the information theory resolution of conventional microscopies is determined by noise of the system and size of the imaging aperture [114].

Although so far the concept has been demonstrated for one-dimensional imaging, both computationally and in a proof-of-principle experiment, it can be readily extended to two- and three-dimensional objects, as well as objects of random shape, and will be very efficient in microscopy of a priori known shapes, such as found in routine tasks of machine vision, smart manufacturing, particle counting for life science applications, etc. The technique does not require labelling of the sample with luminescent materials, nor intense laser illumination, and is resilient to noise. The technique promises far-reaching consequences across a number of disciplines, such as biomedical sciences, materials science and nanotechnology.

Superoscillations beyond optical imaging and metrology

Apart from imaging and metrology, the synthesis of short optical pulses is another emerging direction of superoscillatory technologies. The shortest optical pulses corresponding to the given optical bandwidth are known as bandwidth-limited pulses or Fourier-transform-limited pulses, or more commonly, transform-limited pulses. Bandwidth-limited pulses have a constant phase across all frequencies making up the pulse and such pulses can be generated by mode-locked lasers. For different pulse shapes, the minimum duration-bandwidth product is different, with the Gaussian pulses having a minimum value of 0.441.

If a light wave is constructed from a number of synchronized frequency components, this could create superoscillatory periodic pulsation in time domain containing burst of energy that are shorter than the Fourier-transform-limit for isolated light pulses. This has been demonstrated experimentally by synthesis of four optical frequencies in the red part of the spectrum around the wavelength of 801 nm at frequencies 370.9, 373.2, 375.6 and 377.9 THz with carefully adjusted relative amplitudes of 13, 9, 9 and 13 and mode-locked phase of 0, π, π, 0 using grating based optical pulse shaper [115], Figure 8a. This creates a superoscillatory envelope with a short temporal feature that breaks the temporal Fourier-transform-limit for isolated light pulse, Figure 8b. In the experiment, a temporal feature that is approximately three times narrower than a Fourier-limited Gaussian pulse with the same bandwidth was achieved with a visibility around 30%. Such pulses have been used to demonstrate super-resolution in time domain, where two consecutive pulses were distinguished by mixing them in a nonlinear optical process with the superoscillatory signal, while mixing them with a transform-limited Gaussian pulse of the same bandwidth fails to resolve pulses. The improvement of temporal resolution with superoscillatory pulses was also studied in the context of pulse compression using the Schelkunoff's superdirective antenna design [116]. Remarkably, time domain superoscillatory optical pulses can be used to transmit high-frequency signals through absorbing media [117] or low pass filters [118]. A super-narrow frequency conversion using nonlinear materials with complex, superoscillatory domain structuring has been demonstrated [119].

If superoscillating function can locally oscillate faster than their highest Fourier harmonic, suboscillatory functions exist that oscillate slower than their slowest Fourier harmonic. Suboscillatory functions were introduced in 2017 by Eliezer and Bahabad [120]. For instance, if a function $f(x) = (\cos x + 2i \sin x)^{10}$ is superoscillatory, see Figure 8c, a function $g(x) = (\cos x + \frac{1}{2} i \sin x)^{-10}$ is suboscillatory, see Fig.8d. This function has a lower frequency bound of $k_{min} = 10$. Near $x = 0$ it oscillates at a rate of 0.5 times slower than the slowest component of the spectrum $\cos(10x)$. While superoscillation can lead to superfocusing of light, suboscillations lead to super defocusing of light. Moreover, suboscillatory beams pass around the obstacles without reducing the beam spread in the far-field, which may be useful in dark-field microscopy.

Superoscillation is a general wave phenomenon and can be observed not only with light and acoustic beams, but also with electron De Broglie waves promising interesting applications in high-resolution electron microscopy. Indeed, superoscillatory focusing of electron waves into a central spot that is smaller than the Abbe-Rayleigh diffraction limit was experimentally demonstrated in a scanning electron microscope [121], Figure 8e. a two-zone off-axis computer-generated holographic phase mask was used to generate three diffraction orders with the desired superoscillating electron wave function at the +1 and -1 diffraction orders. A central superoscillatory hotspot with diameter of 228 pm is experimentally measured, which is 66% smaller than the diffraction-limited Airy spot of 670 pm for the given small numerical aperture of the microscope focusing magnetic lens (the electron's De Broglie wavelength is 2 pm at 300keV). The degradation of image contrast in the experiment is mainly attributed to the spatial incoherence of electron source and inelastic scattering in the

supporting substrate of the mask. Here the electron microscope operates essentially in the single-particle regime, supporting the assertion that superoscillations stems from interference of the wave function with itself, similarly to the regime of single photon superoscillations [81], when image of the hotspot is formed by a large number of registration single electron (single photon) events.

Conclusions

In conclusion, in the last few years the phenomenon of superoscillations has evolved from the esoteric effect of wave theory to a practical technology [16,46,122-124]. Here we have revised the basics of the phenomena exploring characteristic features of one and two dimensional superoscillatory functions in particular peculiarities of their spectra. By giving practically important examples we have demonstrated that although the spectrum of the entire function may be band-limited, such functions could locally oscillate faster than the highest harmonic of the spectrum and exhibit area of very rapid phase variation. We have explained how in optics the phenomenon of superoscillations allows for the construction of lenses that can focus light into a hotspot smaller than that is possible by conventional lens. We have examined technologies of binary and continuous superoscillatory intensity and phase masks, metamaterials, superoscillatory lenses and synthesis of superoscillatory fields based on spatial light modulators. We have reviewed the technique for mapping superoscillatory field with deeply subwavelength resolution and have examined the intriguing similarities between the free-space superoscillatory fields and plasmonic fields evanescent on metal surfaces. We have reviewed the optical ruler nano-metrology that exploits the phase singularities of superoscillatory fields as reference points for displacement measurements with potentially femtometric resolution. We have described confocal super-resolution imaging technique with superoscillatory illumination, the way super-resolution images are formed in the band-limited instrument, practical realization of the apparatus and its applications in cell biology. We have explored how the combination of topologically structured superoscillatory light field with artificial intelligence analysis of such field scattered by the nanoscale object offers deeply subwavelength optical resolution. Finally, we have overviewed numerous other applications of superoscillations beyond optical imaging and metrology.

Acknowledgements

The authors are grateful to Edward Rogers, Peter J. S. Smith, Nikitas Papasimakis, Yijie Shen, Bruce Ou, Eng Aik Chan and Carolina Rendon Barraza for discussions and Sruthi Varier for preparation of the manuscript. This work was supported by the Engineering and Physical Sciences Research Council UK (Grants Nos. EP/M009122/1 and EP/T02643X/1), and the Singapore Ministry of Education (Grant No. MOE2016-T3-1-006) and the Agency for Science, Technology and Research (A*STAR) Singapore (Grant No. SERC A1685b0005). Following a period of embargo, the data from this paper can be obtained from the University of Southampton ePrints research repository: https://doi.org/10.5258/SOTON/xxxx.

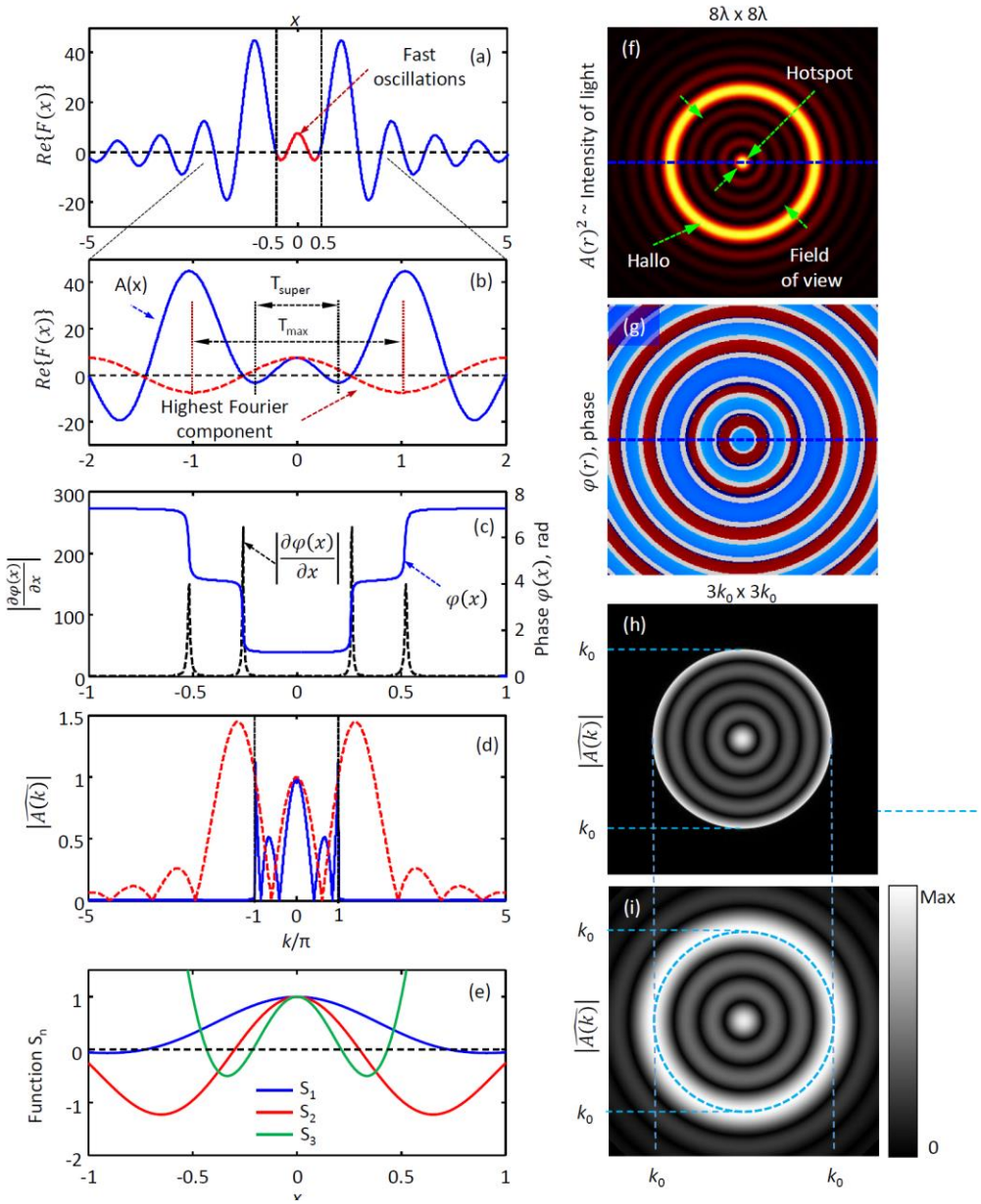

Figure 1. Functions can oscillate faster than their highest Fourier harmonics. An example of a complex superoscillatory function: (a) function profile; (b) zoom-in into its profile near x=0 (blue line); (c) phase of function (blue line) and modulus of its gradient (dashed black line); (d) Modulus of the amplitude of the Fourier spectrum $\widetilde{F(k)} = \widetilde{A(k)} \times \exp\left[i\widetilde{\varphi(k)}\right]$ of function F(x), $\left|\widetilde{A(k)}\right|$ calculated in the x-interval $[-\infty, \infty]$ (solid blue line) and in the x-interval [-0.52, 0.52] (dashed red line), x=0.52 is the zero-point of F(x); (e) The first 3 even-order circular prolate spheroidal functions. A two dimensional superoscillatory focus of coherent light at wavelenghth λ; (f) intensity map; (g) phase map. Plates (h) and (i) compare the band-limited spectrum of the entire superoscillatory hotspot (h) with the spectrum of hotspot within the field of view (i).

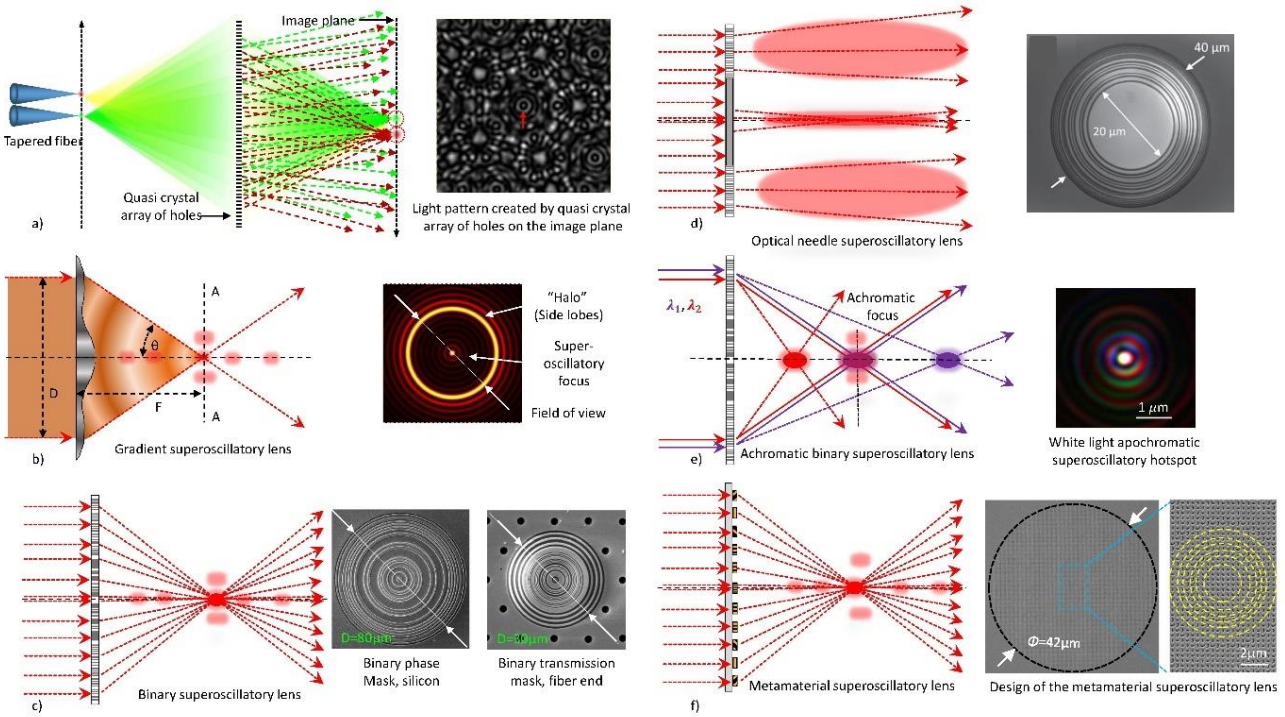

Figure 2. Superoscillatory focusing static lenses. a) Superoscillatory focusing by a quasicrystal array of nano-holes; b) Superoscillatory focusing with a mask with precisely engendered continuous variation of transmissivity and phase retardation; c) Superoscillatory focusing by a binary mask; d) Superoscillatory "optical needle" focusing; e) Achromatic superoscillatory focusing; f) Superoscillatory focusing by a metamaterial superlens.

780

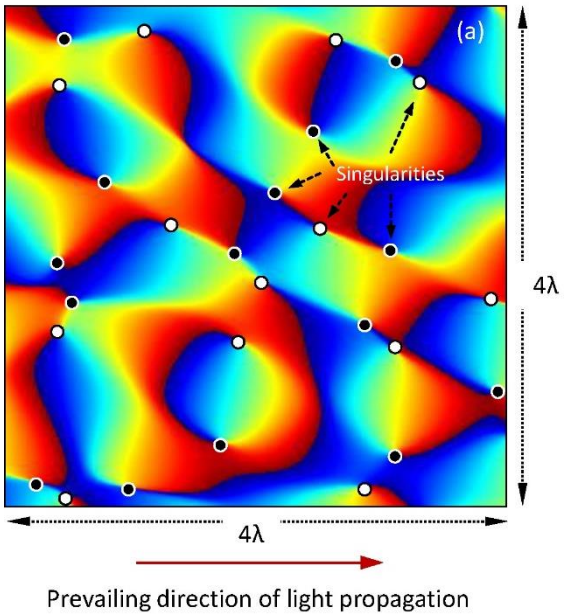

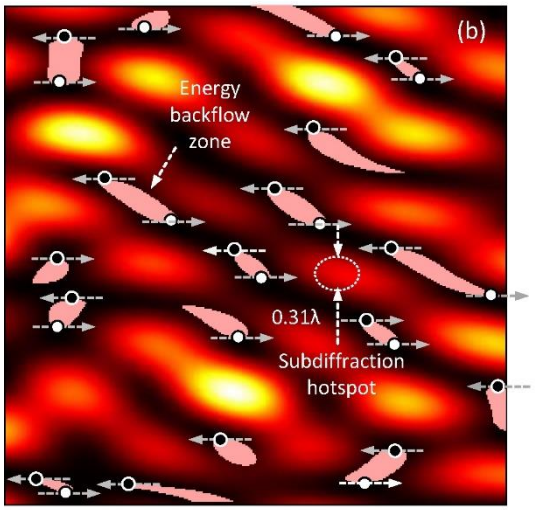

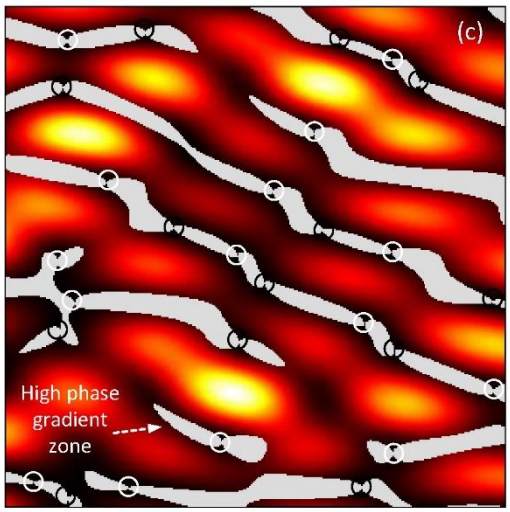

Figure 3. Subwavelength features in complex light fields created by interference of 50 coherent scalar plane waves.

a) The color-coded map of the phase $\varphi(\boldsymbol{r})$ of the resulting electromagnetic field (from blue to red that denote the phase of $-\pi$ and $+\pi$, correspondingly).

b) The color-coded map of intensity $U_0(\boldsymbol{r})$ of the resulting electromagnetic field (white and black corresponding to highest and zero intensity, correspondingly).

c) The intensity map overlapped with the maps of zones (grey) where the phase of the field changes rapidly perpendicular to the prevailing direction of propagation.

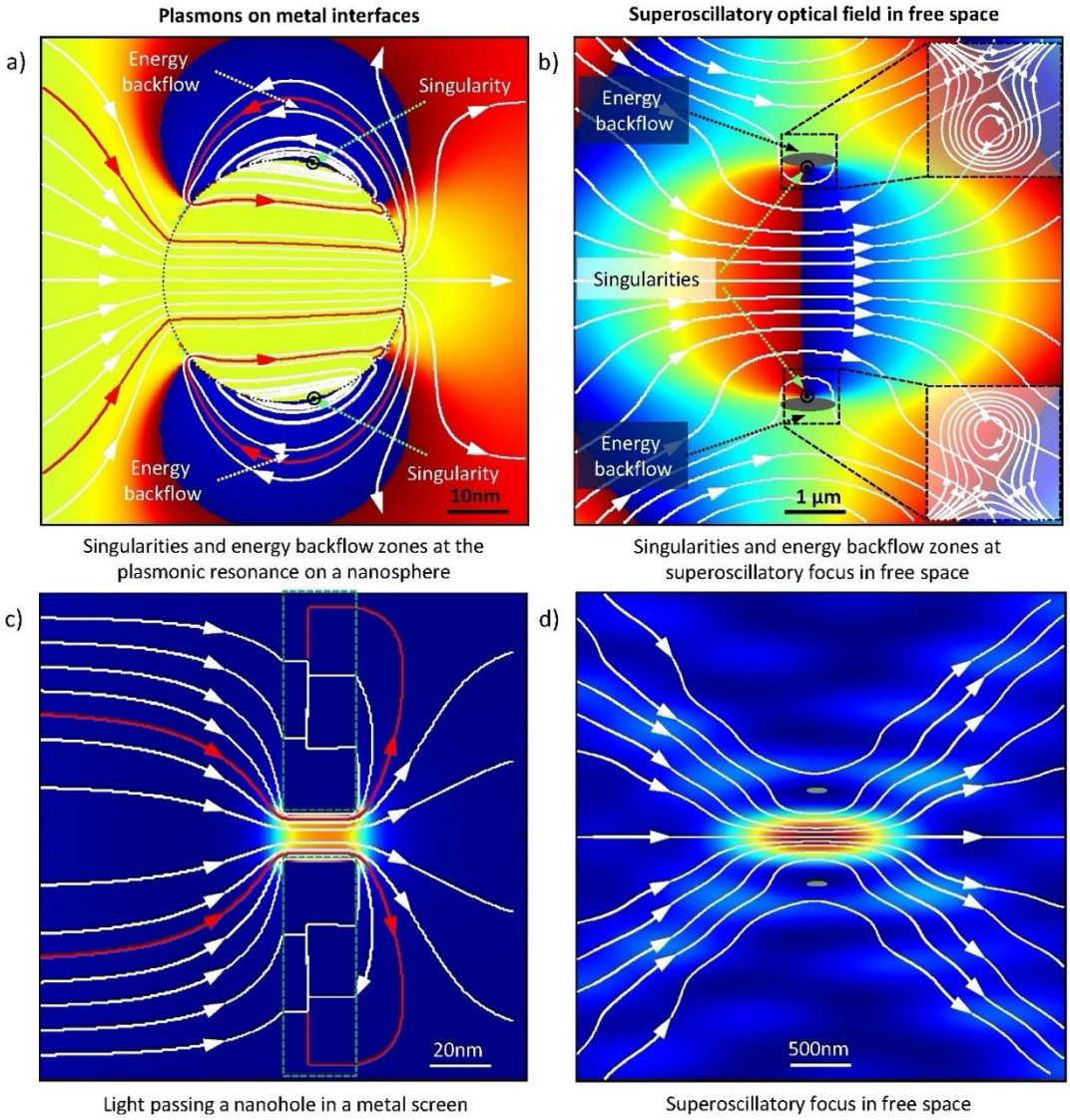

Figure 4. Similarities between plasmonic fields at metal interfaces and superoscillatory field in free space. (a-b) Compare the phase maps (color-coded) and the Poynting vector trajectories (solid lines) of (a) a plane wave propagating from left to right and focused by a silver nanosphere of subwavelength diameter at plasmonic resonance (following reference [98]) and (b) of a free-space field at the superoscillatory hotspot created by diffraction of a plane wave on a one-dimensional metamaterial phase array (also see Figure 7d). In both cases the area of energy concentration is surrounded by singularities and zones of energy backflow "squeezing" the flow of energy into the focus. (c-d) Compare the intensity maps (color-coded) and the Poynting vector trajectories (solid lines) of (c) a light wave passing through a subwavelength hole in a thin plasmonic gold film indicated by a dashed green line [125] and (d) of free-space field at the superoscillatory hotspot. In both cases only a fraction of energy can be channelled into the "sub-diffraction" hotspot, which is a polynomial function $P\left(\sigma/\lambda\right)$ of the ratio between the hotspot diameter σ and the wavelength of light λ.

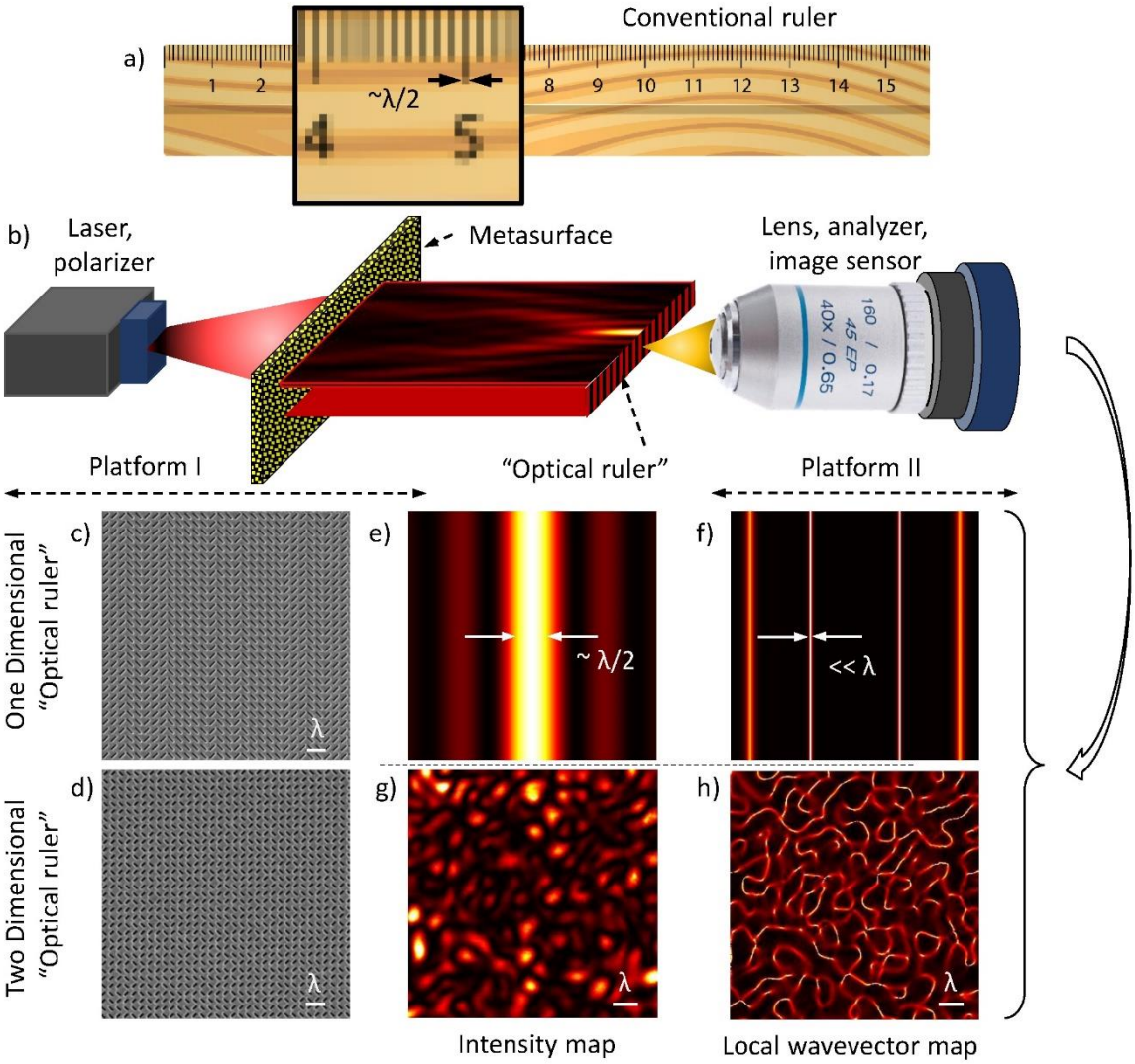

Figure 5. "Optical ruler" metrology. (a) Displacement metrology with conventional ruler relies on the marks on the ruler while its resolution is limited by the imaging lens to about a half of the wavelength. (b) The "optical ruler" metrology measures mutual displacements of two platforms, I and II. (c-h) The "optical ruler" metrology retrieves intensity maps (e & g) and phase gradient maps (f & h) of the field created by one- or two-dimensional metasurfaces (c & d) in free space and uses the zones of strong phase gradient in superoscillatory field as reference marks of the "optical ruler". These zones (lines on maps f & h) are localised orders of magnitude stronger than the intensity hotspot (see maps e & g) offering true nanometric resolution metrology.

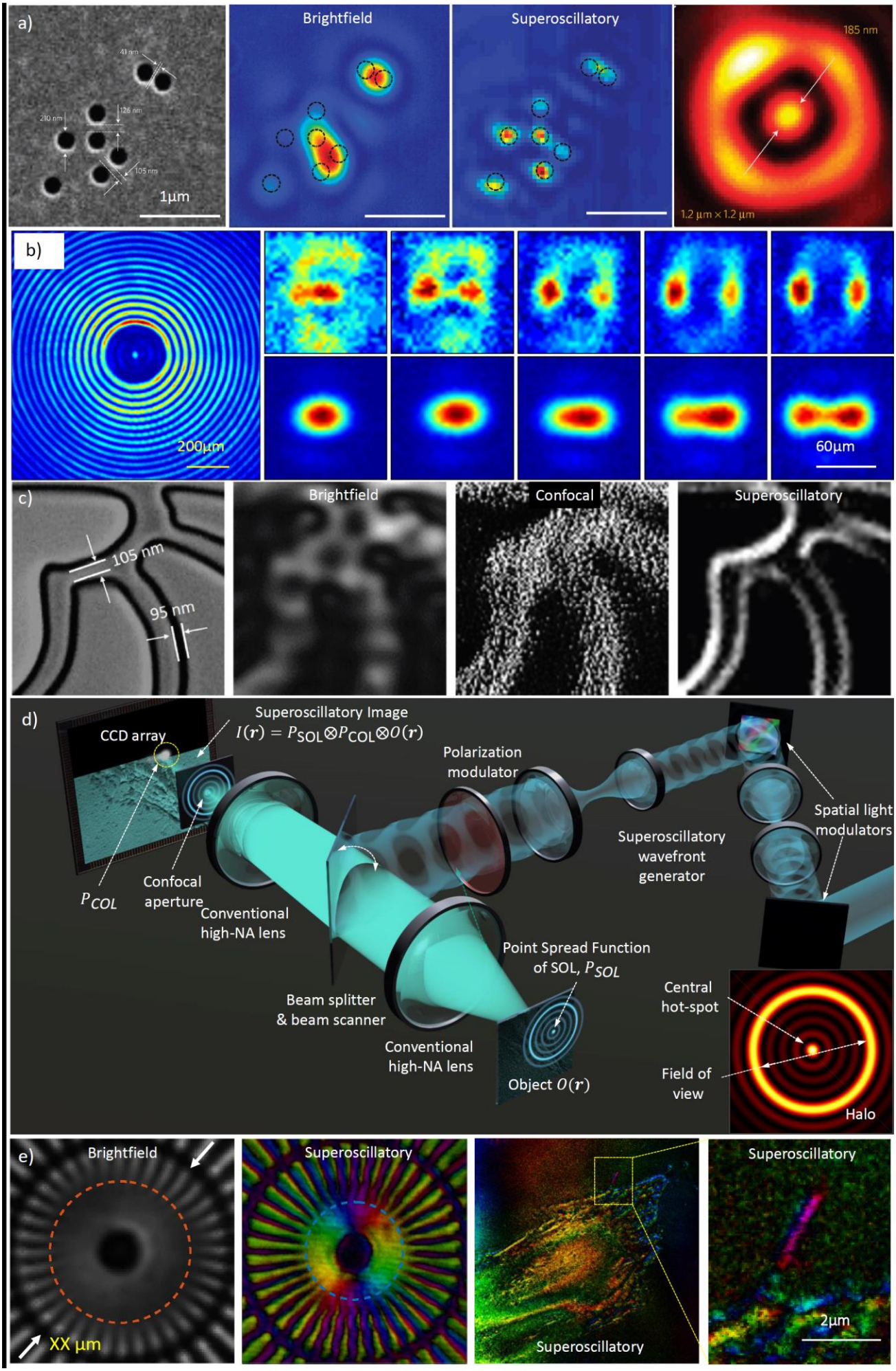
a)
41 nm
126 nm
210 nm
105 nm
1µm
Brightfield
Superoscillatory
185 nm
1.2 µm × 1.2 µm
b)
200µm
60µm
c)
105 nm
95 nm
Brightfield
Confocal
Superoscillatory
d)
CCD array
Superoscillatory Image
$I(\boldsymbol{r}) = P_{SOL} \otimes P_{COL} \otimes O(\boldsymbol{r})$
Polarization modulator
Spatial light modulators
Superoscillatory wavefront generator
P_{COL}
Confocal aperture
Conventional high-NA lens
Point Spread Function of SOL, P_{SOL}
Beam splitter & beam scanner
Conventional high-NA lens
Object $O(\boldsymbol{r})$
Central hot-spot
Field of view
Halo
e)
Brightfield
XX µm
Superoscillatory
Superoscillatory
Superoscillatory
2µm

Figure 6. Superoscillatory Imaging.

Row (a). The first experimental demonstration of super-oscillatory microscope for subwavelength imaging with a resolution up to λ/6 at λ=640 nm [41]: Object (arrays of nanoholes in metal screen); brightfield image; superoscillatory image; the illumination hotspot created by binary superoscillatory lens.

Row (b). An exemplar performance of a SLM based superoscillatory imaging system with far-field working and observation distances [126]. From Left to right: Point Spread Function of the microscope; The comparison of resolving capability of closely spaced apertures: top sub-row, superoscillatory images; bottom sub-row, diffraction-limited images.

Row (c). SEM, brightfield, confocal of superoscillatory images taken of nanostructure at wavelength 405 nm. Superoscillatory image is taken with binary superoscillatory optical needle generator [44].

Row (d). A schematic of the confocal bio-microscope with superoscillatory illumination (following Ref. [85]). The superoscillatory light field is formed by two spatial light modulators and is focused on the object by a conventional lens creating a sub-diffraction illumination hotspot (see inset). A moving semi-transparent mirror is used to scan the hotspot across the sample. The light reflected from the object is detected through a confocal aperture to suppress the effect of halo surrounding the hotspot. The image is itself a superoscillatory function constructed point by point with resolution determined by the size of the hotspot.

Row (e). Images taken with microscope presented on Row (d), from left to right: Conventional brightfield and superoscillatory images of the 36-sector binary Siemens star test object; Dashed red and blue colour lines identify limits of resolution, smaller features of the test object are closer to the centre. A high frame rate live image taken of an unlabelled human bone cell, with zoom-ins detailing a single filopodium: an actin-filled protrusion that guides cell migration.

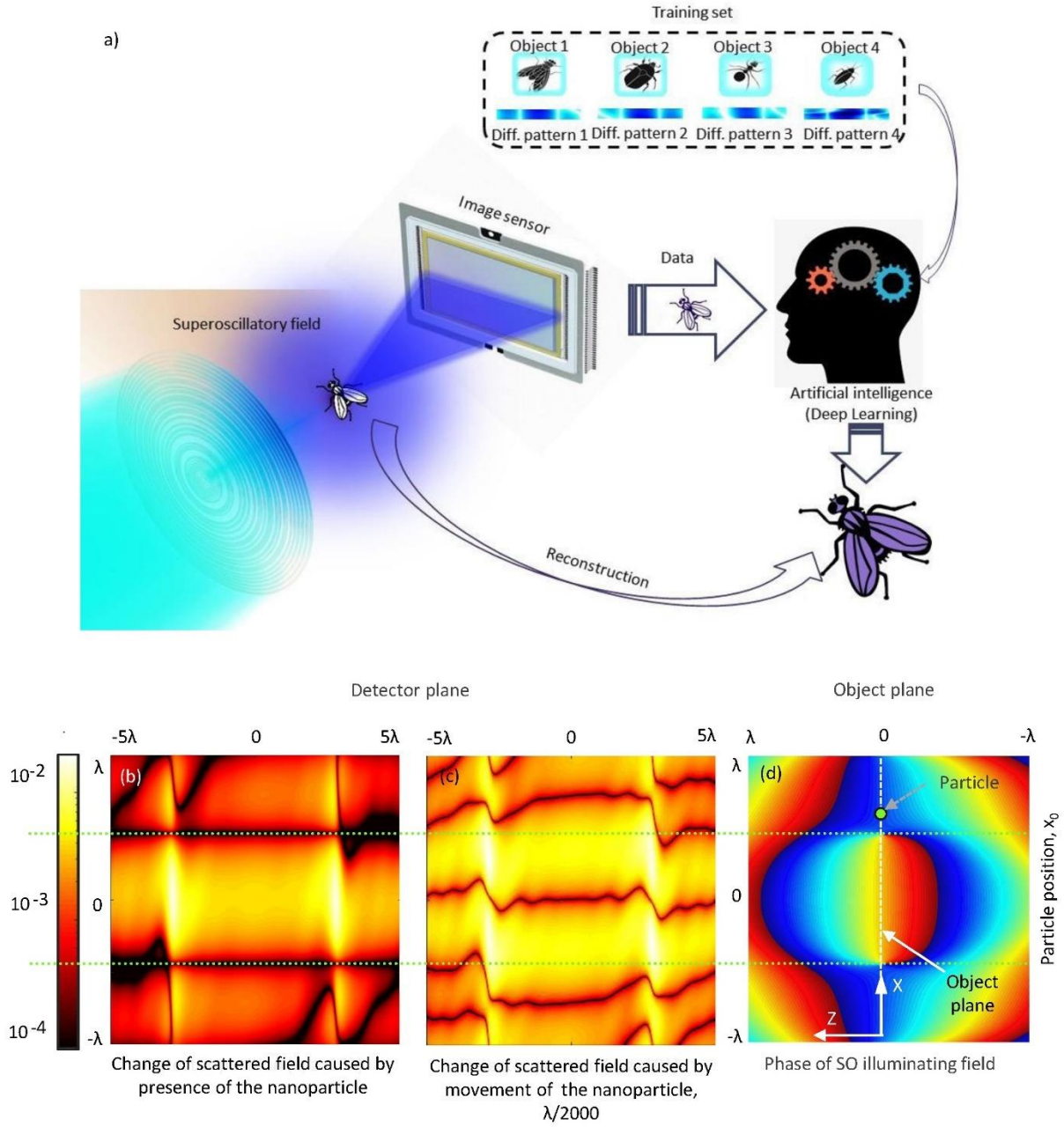

Figure 7. Deeply Subwavelength Topological Imaging with a superoscillatory light field. The intensity profile of the diffraction pattern resulting from scattering of the superoscillatory light field on the imaged object is detected by the image intensity sensor. A number of different diffraction patterns are recorded when the illuminating field is scanned against the object. The artificial intelligence deconvolution programme, trained on a large number of scattering events with a priori known object (numbered 1,2,3,4 …) reconstructs the imaged object from the collected data with high resolution. Plates (b-d) illustrate sensitivity of far-field intensity patterns on presence and position of small absorbing nanoparticle of λ/1000 in size in the image plane. Plate (b) shows normalized change of the scattered field intensity profile caused by presence of the nanoparticle. Plates (c) shows normalized change of the scattered field intensity profile caused by shift of the nanoparticle of λ/2000 along *x* direction. Map (d) shows phase profiles of the illuminating superoscillatory field, where light propagates along the positive z-axis.

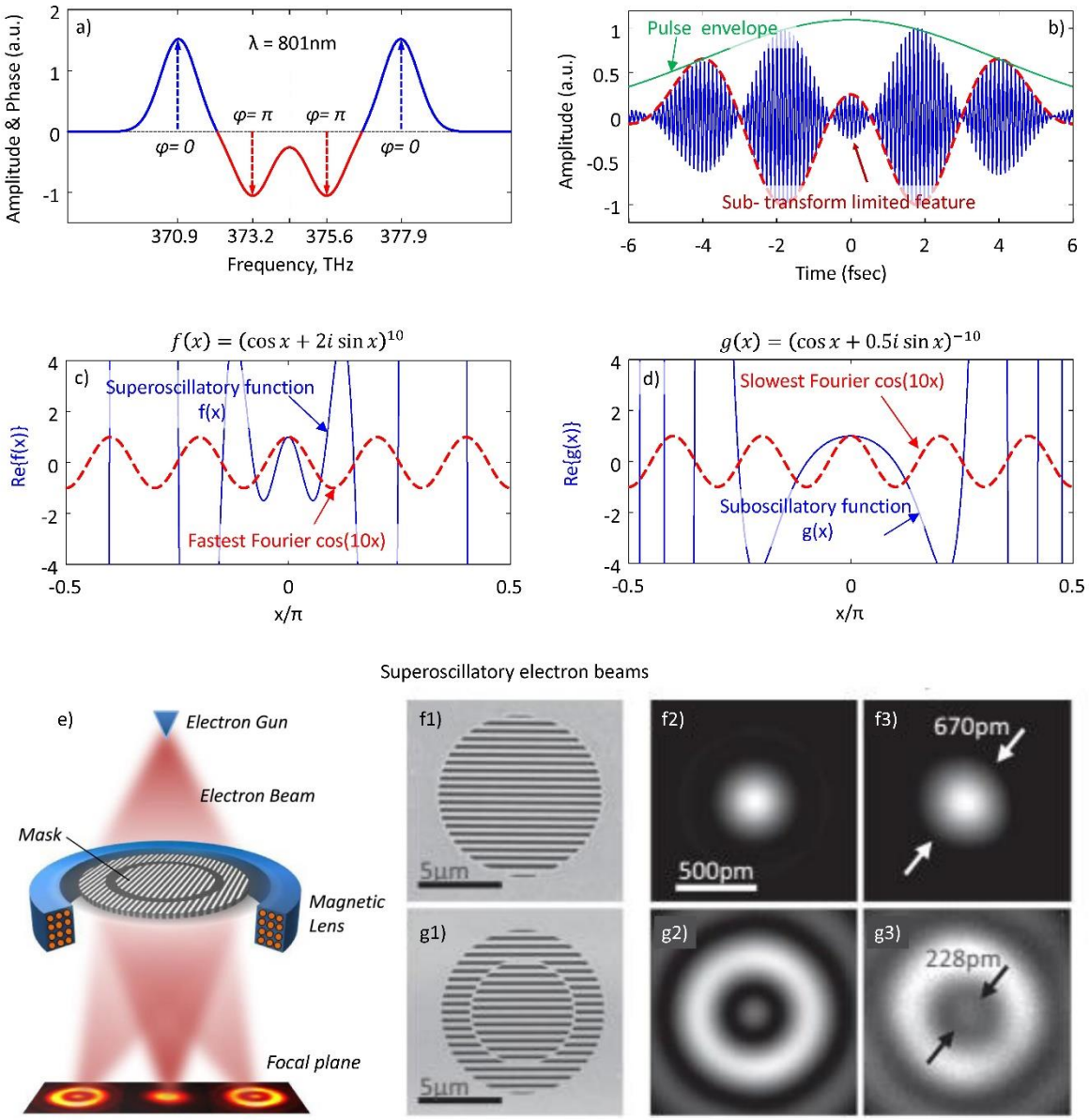

Figure 8. Superoscillations beyond optical imaging and metrology. The spectrum (a) and temporal waveform (b) of the superoscillatory optical beat signal with central wavelength of λ =801 nm, following [115]. (c) A superoscillatory function *f(x)* (blue solid line) that oscillates faster than its highest spectral Fourier component (red dashed line) and (d) a suboscillatory function *g(x)* (blue solid line) that oscillates slower than its slowest spectral Fourier component (red dashed line) near x=0. e) Schematic of electron microscope with binary diffraction masks (f1) or superoscillatory diffraction mask (g1) inserted into the electron beam following [121]. The desired wave function is created in the ±1 diffraction orders. Calculated (f2, g2) and measured (f3, g3) electron hotspots obtained with masks (f1) and (g1) correspondingly. The central hotspot in (g3) is much smaller than allowed by the Abbe-Rayleigh diffraction limit in (f3).

References

1 Atwater, H. A. The promise of plasmonics. *Scientific American* **296**, 56-63, doi:10.1038/scientificamerican0407-56 (2007).

2 Brongersma, M. L. & Shalaev, V. M. The Case for Plasmonics. *Science* **328**, 440-441, doi:10.1126/science.1186905 (2010).

3 Pendry, J. B. Negative refraction makes a perfect lens. *Physical Review Letters* **85**, 3966-3969, doi:10.1103/PhysRevLett.85.3966 (2000).

4 Zhang, X. & Liu, Z. W. Superlenses to overcome the diffraction limit. *Nature Materials* **7**, 435-441, doi:10.1038/nmat2141 (2008).

5 Berry, M. V. & Popescu, S. Evolution of quantum superoscillations and optical superresolution without evanescent waves. *Journal of Physics a-Mathematical and General* **39**, 6965-6977, doi:10.1088/0305-4470/39/22/011 (2006).

6 Berry, M. V. & Moiseyev, N. Superoscillations and supershifts in phase space: Wigner and Husimi function interpretations. *Journal of Physics a-Mathematical and Theoretical* **47**, 315203, doi:10.1088/1751-8113/47/31/315203 (2014).

7 Wang, Q. A simple model of Aharonov-Berry's superoscillations. *Journal of Physics a-Mathematical and General* **29**, 2257-2258 (1996).

8 Ferreira, P., Kempf, A. & Reis, M. Construction of Aharonov-Berry's superoscillations. *Journal of Physics a-Mathematical and Theoretical* **40**, 5141-5147, doi:10.1088/1751-8113/40/19/013 (2007).

9 Huang, F. M. & Zheludev, N. I. Super-Resolution without Evanescent Waves. *Nano Letters* **9**, 1249-1254, doi:10.1021/nl9002014 (2009).

10 Lindberg, J. Mathematical concepts of optical superresolution. *Journal of Optics* **14**, 083001, doi:10.1088/2040-8978/14/8/083001 (2012).

11 Chojnacki, L. & Kempf, A. New methods for creating superoscillations. *Journal of Physics A-Mathematical and Theoretical* **49**, 505203, doi:10.1088/1751-8113/49/50/505203 (2016).

12 Lee, D. G. & Ferreira, P. Direct Construction of Superoscillations. *Ieee Transactions on Signal Processing* **62**, 3125-3134, doi:10.1109/tsp.2014.2321119 (2014).

13 Wong, A. M. H. & Eleftheriades, G. V. Adaptation of Schelkunoff's Superdirective Antenna Theory for the Realization of Superoscillatory Antenna Arrays. *Ieee Antennas and Wireless Propagation Letters* **9**, 315-318, doi:10.1109/lawp.2010.2047710 (2010).

14 Chremmos, I. & Fikioris, G. Superoscillations with arbitrary polynomial shape. *Journal of Physics a-Mathematical and Theoretical* **48**, 265204, doi:10.1088/1751-8113/48/26/265204 (2015).

15 Smith, M. K. & Gbur, G. Mathematical method for designing superresolution lenses using superoscillations. *Optics Letters* **45**, 1854-1857, doi:10.1364/ol.388252 (2020).

16 Rogers, K. S. R., E. T. F. Realising superoscillations: A review of mathematical tools and their application. *Journal of Physics Photonics* **2**, 042004 (2020).

17 Zheludev, N. I. What diffraction limit? *Nature Materials* **7**, 420-422, doi:10.1038/nmat2163 (2008).

18 Karoui, A. & Moumni, T. Spectral analysis of the finite Hankel transform and circular prolate spheroidal wave functions. *Journal of Computational and Applied Mathematics* **233**, 315-333, doi:10.1016/j.cam.2009.07.037 (2009).

19 Ferreira, P. & Kempf, A. Superoscillations: Faster than the Nyquist rate. *Ieee Transactions on Signal Processing* **54**, 3732-3740, doi:10.1109/tsp.2006.877642 (2006).

20 Kempf, A. & Ferreira, P. Unusual properties of superoscillating particles. *Journal of Physics a-Mathematical and General* **37**, 12067-12076, doi:10.1088/0305-4470/37/50/009 (2004).

21 Tang, E., Garg, L. & Kempf, A. Scaling properties of superoscillations and the extension to periodic signals. *Journal of Physics a-Mathematical and Theoretical* **49**, 335202, doi:10.1088/1751-8113/49/33/335202 (2016).

22 Kempf, A. Black holes, bandwidths and Beethoven. *Journal of Mathematical Physics* **41**, 2360-2374, doi:10.1063/1.533244 (2000).

23 Shannon, C. E. A mathematical theory of communication. *Bell System Technical Journal* **27**, 623-656, doi:10.1002/j.1538-7305.1948.tb00917.x (1948).

24 Aharonov, Y., Albert, D. Z. & Vaidman, L. How the result of a measurement of a component of the spin of a spin-1/2 particle can turn out to be 100. *Physical Review Letters* **60**, 1351-1354, doi:10.1103/PhysRevLett.60.1351 (1988).
25 Berry, M. V. & Shukla, P. Typical weak and superweak values. *Journal of Physics a-Mathematical and Theoretical* **43**, 354024, doi:10.1088/1751-8113/43/35/354024 (2010).
26 Vigoureux, J. M., Dhooge, L. & Vanlabeke, D. Quantization of Evanescent Electromagnetic-Waves - Momentum of the Electromagnetic-Field Very Close to a Dielectric Medium. *Physical Review A* **21**, 347-355, doi:DOI 10.1103/PhysRevA.21.347 (1980).
27 Berry, M. V. Superluminal speeds for relativistic random waves. *Journal of Physics a-Mathematical and Theoretical* **45**, 185308, doi:10.1088/1751-8113/45/18/185308 (2012).
28 Hosten, O. & Kwiat, P. Observation of the spin Hall effect of light via weak measurements. *Science* **319**, 787-790, doi:10.1126/science.1152697 (2008).
29 Toraldo Di Francia, G. Super-gain antennas and optical resolving power. *Il Nuovo Cimento* **9**, 13 (1952).
30 Schelkunoff, S. A. A mathematical theory of linear arrays. *Bell System Technical Journal* **22**, 80-107, doi:10.1002/j.1538-7305.1943.tb01306.x (1943).
31 Leiserson, I., Lipson, S. G. & Sarafis, V. Superresolution in far-field imaging. *Optics Letters* **25**, 209-211, doi:10.1364/ol.25.000209 (2000).
32 Leizerson, I., Lipson, S. G. & Sarafis, V. Superresolution in far-field imaging. *Journal of the Optical Society of America a-Optics Image Science and Vision* **19**, 436-443, doi:10.1364/josaa.19.000436 (2002).
33 Huang, F. M., Zheludev, N., Chen, Y. F. & de Abajo, F. J. G. Focusing of light by a nanohole array. *Applied Physics Letters* **90**, 091119, doi:10.1063/1.2710775 (2007).
34 Huang, F. M., Chen, Y., de Abajo, F. J. G. & Zheludev, N. I. Optical super-resolution through super-oscillations. *Journal of Optics a-Pure and Applied Optics* **9**, S285-S288, doi:10.1088/1464-4258/9/9/s01 (2007).
35 Rogers, K. S., Bourdakos, K. N., Yuan, G. H., Mahajan, S. & Rogers, E. T. F. Optimising superoscillatory spots for far-field super-resolution imaging. *Optics Express* **26**, 8095-8112, doi:10.1364/oe.26.008095 (2018).
36 Maznev, A. A. & Wright, O. B. Upholding the diffraction limit in the focusing of light and sound. *Wave Motion* **68**, 182-189, doi:10.1016/j.wavemoti.2016.09.012 (2017).
37 Padgett, M. On the focussing of light, as limited by the uncertainty principle. *Journal of Modern Optics* **55**, 3083-3089, doi:10.1080/09500340802272365 (2008).
38 Huang, F. M., Kao, T. S., Fedotov, V. A., Chen, Y. F. & Zheludev, N. I. Nanohole array as a lens. *Nano Letters* **8**, 2469-2472, doi:10.1021/nl801476v (2008).
39 Oreopoulos, J., Berman, R. & Browne, M. in *Quantitative Imaging in Cell Biology* Vol. 123 *Methods in Cell Biology* (eds J. C. Waters & T. Wittmann) 153-175 (2014).
40 Wang, Q. *et al.* Reconfigurable phase-change photomask for grayscale photolithography. *Applied Physics Letters* **110**, 201110, doi:10.1063/1.4983198 (2017).
41 Rogers, E. T. F. *et al.* A super-oscillatory lens optical microscope for subwavelength imaging. *Nature Materials* **11**, 432-435, doi:10.1038/nmat3280 (2012).
42 Chen, G. *et al.* Generation of a sub-diffraction hollow ring by shaping an azimuthally polarized wave. *Scientific Reports* **6**, 37776, doi:10.1038/srep37776 (2016).
43 Wu, Z. X. *et al.* Generating a three-dimensional hollow spot with sub-diffraction transverse size by a focused cylindrical vector wave. *Optics Express* **26**, 7866-7875, doi:10.1364/oe.26.007866 (2018).
44 Qin, F. *et al.* A Supercritical Lens Optical Label-Free Microscopy: Sub-Diffraction Resolution and Ultra-Long Working Distance. *Advanced Materials* **29**, 1602721, doi:10.1002/adma.201602721 (2017).
45 Zhu, X. F. *et al.* Supercritical lens array in a centimeter scale patterned with maskless UV lithography. *Optics Letters* **45**, 1798-1801, doi:10.1364/ol.389702 (2020).
46 Chen, G., Wen, Z. Q. & Qiu, C. W. Superoscillation: from physics to optical applications. *Light-Science & Applications* **8**, 56, doi:10.1038/s41377-019-0163-9 (2019).

47 Legaria, S., Pacheco-Pena, V. & Beruete, M. Super-Oscillatory Metalens at Terahertz for Enhanced Focusing with Reduced Side Lobes. *Photonics* **5**, 56, doi:10.3390/photonics5040056 (2018).

48 Liu, T., Shen, T., Yang, S. M. & Jiang, Z. D. Subwavelength focusing by binary multi-annularplates: design theory and experiment. *Journal of Optics* **17**, 035610, doi:10.1088/2040-8978/17/3/035610 (2015).

49 Chen, G. *et al.* Far-field sub-diffraction focusing lens based on binary amplitude-phase mask for linearly polarized light. *Optics Express* **24**, 11002-11008, doi:10.1364/oe.24.011002 (2016).

50 Chen, G. *et al.* Super-oscillatory focusing of circularly polarized light by ultra-long focal length planar lens based on binary amplitude-phase modulation. *Scientific Reports* **6**, 29068, doi:10.1038/srep29068 (2016).

51 Li, M. Y., Li, W. L., Li, H. Y., Zhu, Y. C. & Yu, Y. T. Controllable design of super-oscillatory lenses with multiple sub-diffraction-limit foci. *Scientific Reports* **7**, 1335, doi:10.1038/s41598-017-01492-y (2017).

52 Huang, K. *et al.* Optimization-free superoscillatory lens using phase and amplitude masks. *Laser & Photonics Reviews* **8**, 152-157, doi:10.1002/lpor.201300123 (2014).

53 Wu, Z. X. *et al.* Optimization-free approach or generating sub-diffraction quasi-non-diffracting beams. *Optics Express* **26**, 16585-16599, doi:10.1364/oe.26.016585 (2018).

54 Rogers, E. T. F. & Zheludev, N. I. Optical super-oscillations: sub-wavelength light focusing and super-resolution imaging. *Journal of Optics* **15**, 094008, doi:10.1088/2040-8978/15/9/094008 (2013).

55 Huang, K. *et al.* Ultrahigh-capacity non-periodic photon sieves operating in visible light. *Nature Communications* **6**, 7059, doi:10.1038/ncomms8059 (2015).

56 Qin, F. *et al.* Shaping a Subwavelength Needle with Ultra-long Focal Length by Focusing Azimuthally Polarized Light. *Scientific Reports* **5**, 09977, doi:10.1038/srep09977 (2015).

57 Yu, Y. T., Li, W. L., Li, H. Y., Li, M. Y. & Yuan, W. Z. An Investigation of Influencing Factors on Practical Sub-Diffraction-Limit Focusing of Planar Super-Oscillation Lenses. *Nanomaterials* **8**, 185, doi:10.3390/nano8040185 (2018).

58 Yuan, G. H., Rogers, E. T. F. & Zheludev, N. I. Achromatic super-oscillatory lenses with sub-wavelength focusing. *Light-Science & Applications* **6**, e17036, doi:10.1038/lsa.2017.36 (2017).

59 Wang, Z. *et al.* Exciton-enabled meta-optics in two-dimensional transition metal dichalcogenides. *Nano Letters* **20**, 7964-7972 (2020).

60 Yuan, G. H., Lin, Y. H., Tsai, D. P. & Zheludev, N. I. Superoscillatory quartz lens with effective numerical aperture greater than one. *Applied Physics Letters* **117**, 021106, doi:10.1063/5.0013823 (2020).

61 Li, W. L., Yu, Y. T. & Yuan, W. Z. Flexible focusing pattern realization of centimeter- scale planar super-oscillatory lenses in parallel fabrication. *Nanoscale* **11**, 311-320, doi:10.1039/c8nr07985d (2019).

62 Wang, Q. *et al.* Optically reconfigurable metasurfaces and photonic devices based on phase change materials. *Nature Photonics* **10**, 60-65, doi:10.1038/nphoton.2015.247 (2016).

63 Yu, N. F. & Capasso, F. Flat optics with designer metasurfaces. *Nature Materials* **13**, 139-150, doi:10.1038/nmat3839 (2014).

64 Khorasaninejad, M. *et al.* Metalenses at visible wavelengths: Diffraction-limited focusing and subwavelength resolution imaging. *Science* **352**, 1190-1194, doi:10.1126/science.aaf6644 (2016).

65 Roy, T., Yuan, G. H., Rogers, E. T. F., Zheludev, N. I. & Ieee. in *2014 Conference on Lasers and Electro-Optics Conference on Lasers and Electro-Optics* FW3K.3 (2014).

66 Yuan, G. H., Rogers, E. T. F., Roy, T., Shen, Z. X. & Zheludev, N. I. Flat super-oscillatory lens for heat-assisted magnetic recording with sub-50nm resolution. *Optics Express* **22**, 6428-6437, doi:10.1364/oe.22.006428 (2014).

67 Banerji, S., Meem, M., Majumder, A., Sensale-Rodriguez, B. & Menon, R. Extreme-depth-of-focus imaging with a flat lens. *Optica* **7**, 214-217, doi:10.1364/optica.384164 (2020).

68 Oseen, C. W. Einstein's pinprick radiation and Maxwell's equations. *Annalen Der Physik* **69**, 202-204 (1922).

69 Rogers, E. T. F. *et al.* Super-oscillatory optical needle. *Applied Physics Letters* **102**, 031108, doi:10.1063/1.4774385 (2013).

70 Roy, T., Rogers, E. T. F., Yuan, G. H. & Zheludev, N. I. Point spread function of the optical needle super-oscillatory lens. *Applied Physics Letters* **104**, 231109, doi:10.1063/1.4882246 (2014).

71 Yuan, G. H. *et al.* Planar super-oscillatory lens for sub-diffraction optical needles at violet wavelengths. *Scientific Reports* **4**, 6333, doi:10.1038/srep06333 (2014).
72 Diao, J. S., Yuan, W. Z., Yu, Y. T., Zhu, Y. C. & Wu, Y. Controllable design of super-oscillatory planar lenses for sub-diffraction-limit optical needles. *Optics Express* **24**, 1924-1933, doi:10.1364/oe.24.001924 (2016).
73 Chen, G. *et al.* Planar binary-phase lens for super-oscillatory optical hollow needles. *Scientific Reports* **7**, 4697, doi:10.1038/s41598-017-05060-2 (2017).
74 Kryder, M. H. *et al.* Heat Assisted Magnetic Recording. *Proceedings of the Ieee* **96**, 1810-1835, doi:10.1109/jproc.2008.2004315 (2008).
75 Yuan, G. H. *et al.* in *2013 Conference on Lasers and Electro-Optics Conference on Lasers and Electro-Optics* QM1B.8 (2013).
76 Yuan, G. H., Rogers, K. S., Rogers, E. T. F. & Zheludev, N. I. Far-Field Superoscillatory Metamaterial Superlens. *Physical Review Applied* **11**, 064016, doi:10.1103/PhysRevApplied.11.064016 (2019).
77 Papakostas, A. *et al.* Optical manifestations of planar chirality. *Physical Review Letters* **90**, 107404, doi:10.1103/PhysRevLett.90.107404 (2003).
78 Yu, N. F. *et al.* Light Propagation with Phase Discontinuities: Generalized Laws of Reflection and Refraction. *Science* **334**, 333-337, doi:10.1126/science.1210713 (2011).
79 Tang, D. L. *et al.* Ultrabroadband superoscillatory lens composed by plasmonic metasurfaces for subdiffraction light focusing. *Laser & Photonics Reviews* **9**, 713-719, doi:10.1002/lpor.201500182 (2015).
80 Li, Z. *et al.* Achromatic Broadband Super-Resolution Imaging by Super-Oscillatory Metasurface. *Laser & Photonics Reviews* **12**, 180064, doi:10.1002/lpor.201800064 (2018).
81 Yuan, G. H. *et al.* Quantum super-oscillation of a single photon. *Light-Science & Applications* **5**, e16127, doi:10.1038/lsa.2016.127 (2016).
82 Rueckner, W. & Peidle, J. Young's double-slit experiment with single photons and quantum eraser. *American Journal of Physics* **81**, 951-958, doi:10.1119/1.4819882 (2013).
83 Huignard, J. P. Spatial light modulators and their applications. *Journal of Optics-Nouvelle Revue D Optique* **18**, 181-186, doi:10.1088/0150-536x/18/4/003 (1987).
84 Maurer, C., Jesacher, A., Bernet, S. & Ritsch-Marte, M. What spatial light modulators can do for optical microscopy. *Laser & Photonics Reviews* **5**, 81-101, doi:10.1002/lpor.200900047 (2011).
85 Rogers, E. T. F. Q., S.; Rogers, K. S.; Newman, T. A.; Smith, P. J. S.; Zheludev, N. I. Far-field Unlabeled Super-Resolution Imaging with Superoscillatory Illumination. *APL Photonics* **5**, 066107, doi:10.1063/1.5144918 (2020).
86 Singh, B. K., Nagar, H., Roichman, Y. & Arie, A. Particle manipulation beyond the diffraction limit using structured super-oscillating light beams. *Light-Science & Applications* **6**, e17050, doi:10.1038/lsa.2017.50 (2017).
87 Singh, B. K., Nagar, H., Roichman, Y. & Arie, A. in *Optical Trapping and Optical Micromanipulation Xv* Vol. 10723 *Proceedings of SPIE* (eds K. Dholakia & G. C. Spalding) 1072303 (2018).
88 Johnson, C. W. *et al.* Exact design of complex amplitude holograms for producing arbitrary scalar fields. *Optics Express* **28**, 17334-17346, doi:10.1364/oe.393224 (2020).
89 Wan, Z. S., Wang, Z. Y., Yang, X. L., Shen, Y. J. & Fu, X. Digitally tailoring arbitrary structured light of generalized ray-wave duality. *Optics Express* **28**, 31043-31056, doi:10.1364/oe.400587 (2020).
90 Ruan, D. S. *et al.* Realizing a terahertz far-field sub-diffraction optical needle with sub-wavelength concentric ring structure array. *Applied Optics* **57**, 7905-7909, doi:10.1364/ao.57.007905 (2018).
91 Yang, M. Y. *et al.* Subdiffraction focusing of total electric fields of terahertz wave. *Optics Communications* **458**, 124764, doi:10.1016/j.optcom.2019.124764 (2020).
92 Shen, Y. X. *et al.* Ultrasonic super-oscillation wave-packets with an acoustic meta-lens. *Nature Communications* **10**, 3411, doi:10.1038/s41467-019-11430-3 (2019).
93 Hyun, J. *et al.* Realization of an ultrathin acoustic lens for subwavelength focusing in the megasonic range. *Scientific Reports* **8**, 9131, doi:10.1038/s41598-018-27312-5 (2018).

94 Berry, M. V. & Dennis, M. R. Natural superoscillations in monochromatic waves in D dimensions. *Journal of Physics a-Mathematical and Theoretical* **42**, 022003, doi:10.1088/1751-8113/42/2/022003 (2009).
95 Dennis, M. R., Hamilton, A. C. & Courtial, J. Superoscillation in speckle patterns. *Optics Letters* **33**, 2976-2978, doi:10.1364/ol.33.002976 (2008).
96 Berry, M. V. Quantum backflow, negative kinetic energy, and optical retro-propagation. *Journal of Physics a-Mathematical and Theoretical* **43**, 415302, doi:10.1088/1751-8113/43/41/415302 (2010).
97 Yuan, G. H., Rogers, E. T. F. & Zheludev, N. I. "Plasmonics" in free space: observation of giant wavevectors, vortices, and energy backflow in superoscillatory optical fields. *Light-Science & Applications* **8**, 2, doi:10.1038/s41377-018-0112-z (2019).
98 Bashevoy, M. V., Fedotov, V. A. & Zheludev, N. I. Optical whirlpool on an absorbing metallic nanoparticle. *Optics Express* **13**, 8372-8379, doi:10.1364/opex.13.008372 (2005).
99 Yuan, G. H. & Zheludev, N. I. Detecting nanometric displacements with optical ruler metrology. *Science* **364**, 771-775, doi:10.1126/science.aaw7840 (2019).
100 Nye, J. F., Berry, M. V. & Walford, M. E. R. Measuring change in thickness of antarctic ice sheet. *Nature-Physical Science* **240**, 7-9, doi:10.1038/physci240007a0 (1972).
101 Betzig, E. *et al.* Imaging intracellular fluorescent proteins at nanometer resolution. *Science* **313**, 1642-1645, doi:10.1126/science.1127344 (2006).
102 Blom, H. & Widengren, J. Stimulated Emission Depletion Microscopy. *Chemical Reviews* **117**, 7377-7427, doi:10.1021/acs.chemrev.6b00653 (2017).
103 Wang, C. T. *et al.* Super-resolution optical telescopes with local light diffraction shrinkage. *Scientific Reports* **5**, doi:10.1038/srep18485 (2015).
104 Rogers, E. T. F. *et al.* New Super-Oscillatory Technology for Unlabelled Super-Resolution Cellular Imaging with Polarisation Contrast. *Biophysical Journal* **112**, 186A-186A, doi:10.1016/j.bpj.2016.11.1031 (2017).
105 Thibault, P. & Elser, V. X-Ray Diffraction Microscopy. *Annu Rev Conden Ma P* **1**, 237-255, doi:10.1146/annurev-conmatphys-070909-104034 (2010).
106 Gazit, S., Szameit, A., Eldar, Y. C. & Segev, M. Super-resolution and reconstruction of sparse sub-wavelength images. *Optics Express* **17**, 23920-23946, doi:10.1364/Oe.17.023920 (2009).
107 Rivenson, Y. *et al.* Deep learning microscopy. *Optica* **4**, 1437-1443, doi:10.1364/optica.4.001437 (2017).
108 Ouyang, W., Aristov, A., Lelek, M., Hao, X. & Zimmer, C. Deep learning massively accelerates super-resolution localization microscopy. *Nature Biotechnology* **36**, 460-468, doi:10.1038/nbt.4106 (2018).
109 Wang, H. D. *et al.* Deep learning enables cross-modality super-resolution in fluorescence microscopy. *Nature Methods* **16**, 103-110, doi:10.1038/s41592-018-0239-0 (2019).
110 Piccinotti, D., MacDonald, K. F., Gregory, S., Youngs, I. & Zheludev, N. I. Artificial intelligence for photonics and photonic materials. *Reports on Progress in Physics* **84**, 012401, doi:10.1088/1361-6633/abb4c7 (2020).
111 Pu, T. O., J. Y.; Papasimakis, N.; Zheludev N. I. Label-free deeply subwavelength optical microscopy. *Applied Physics Letters* **116**, 131105 (2020).
112 Rendon-Barraza, C. C., E. A.; Yuan, G. H.; Adamo, G.; Pu, T.; Zheludev, N. I. Optical metrology of sub-wavelength objects enabled by artificial intelligence. doi:http://arxiv.org/abs/2005.04905 (2020).
113 Pu, T. O., J. Y.; Savinov, V.; Yuan, G. H.; Papasimakis, N.; Zheludev, N. I. Unlabeled far-field deeply subwavelength topological microscopy (DSTM). *Advanced Science* **2020**, 2002886 (2020).
114 Narimanov, E. Resolution limit of label-free far-field microscopy. *Advanced Photonics* **1**, 056003 (2019).
115 Eliezer, Y., Hareli, L., Lobachinsky, L., Froim, S. & Bahabad, A. Breaking the Temporal Resolution Limit by Superoscillating Optical Beats. *Physical Review Letters* **119**, 043903, doi:10.1103/PhysRevLett.119.043903 (2017).

116 Wong, A. M. H. & Eleftheriades, G. V. Temporal Pulse Compression Beyond the Fourier Transform Limit. *Ieee Transactions on Microwave Theory and Techniques* **59**, 2173-2179, doi:10.1109/tmtt.2011.2160961 (2011).
117 Eliezer, Y. & Bahabad, A. Super-transmission: the delivery of superoscillations through the absorbing resonance of a dielectric medium. *Optics Express* **22**, 31212-31226, doi:10.1364/oe.22.031212 (2014).
118 Zarkovsky, S. B.-E., Y.; Schwartz, M. Transmission of Superoscillations. *Scientific Reports* **10**, 5893 (2020).
119 Remez, R. & Arie, A. Super-narrow frequency conversion. *Optica* **2**, 472-475, doi:10.1364/optica.2.000472 (2015).
120 Eliezer, Y. & Bahabad, A. Super defocusing of light by optical sub-oscillations. *Optica* **4**, 440-446, doi:10.1364/optica.4.000440 (2017).
121 Remez, R. *et al.* Superoscillating electron wave functions with subdiffraction spots. *Physical Review A* **95**, 031802(R), doi:10.1103/PhysRevA.95.031802 (2017).
122 Huang, K. *et al.* Planar Diffractive Lenses: Fundamentals, Functionalities, and Applications. *Advanced Materials* **30**, 1704556, doi:10.1002/adma.201704556 (2018).
123 Berry, M. *et al.* Roadmap on superoscillations. *Journal of Optics* **21**, 053002, doi:10.1088/2040-8986/ab0191 (2019).
124 Gbur, G. Using superoscillations for superresolved imaging and subwavelength focusing. *Nanophotonics* **8**, 205-225, doi:10.1515/nanoph-2018-0112 (2019).
125 Piccinotti, D. *et al.* Optical Response of Nanohole Arrays Filled with Chalcogenide Low-Epsilon Media. *Advanced Optical Materials* **6**, 1800395, doi:10.1002/adom.201800395 (2018).
126 Wong, A. M. H. & Eleftheriades, G. V. An Optical Super-Microscope for Far-field, Real-time Imaging Beyond the Diffraction Limit. *Scientific Reports* **3**, doi:10.1038/srep01715 (2013).